Dynamic Analysis of an Exponentially Decaying Foundation on the Response of Non-Uniform Damped Rayleigh Beam under Harmonic Moving Load with General Boundary Conditions

Abstract

This study investigates the dynamic response of a non-uniform damped Rayleigh beam on an exponentially decaying foundation subjected to a harmonic moving load with general boundary conditions. The governing equation, a fourth-order non-homogeneous partial differential equation with variable coefficients, is discretized using the Generalized Galerkin Method. Two cases are examined: moving force and moving mass. Closed-form solutions are obtained for the moving force case using Laplace transform in conjuction with convolution theorem. For the moving mass case, the Struble asymptotic method cannot simplify the equation for the moving mass case due to the variable load magnitude, and thus, Runge-Kutta method of order four (RK4) is employed to obtain a numerical solution. Analytical and numerical solutions are compared for validation of accuracy of the Runge-kutta scheme and found compared favourably. The effects of some key structural parameters on dynamic behavior are examined, and resonance conditions are established

Keywords: Damped Rayleigh beam, Exponentially decaying foundation, Harmonic moving load and Generalized Galerkin Method

1 Introduction

The dynamic analysis of non-uniform beams has garnered significant attention in recent years due to its widespread applications in civil, mechanical, and aerospace engineering. A particular type of beam that has been extensively studied is the Rayleigh beam, which accounts for the effects of rotatory inertia and shear deformation, has become a widely accepted model for understanding beam behaviour. Studying how structural components on foundations react dynamically to shifting loads is essential because it can help us better understand dynamic properties in various fields, such as mechanical engineering, aerospace, and transportation infrastructure. The works of several researchers, including [1],[2],[3],[4],[5] and [6], have made significant contributions to this field.

Non-uniform Rayleigh beams, characterized by varying cross-sectional properties along their length, provide a more accurate representation of real-life dynamic structures than traditional uniform Rayleigh

beams. Accounting for non-uniformities in geometry, material properties, or both, allows for a more realistic modeling of structures such as bridges, buildings, and aircraft wings. Studies have shown that neglecting these non-uniformities can lead to significant errors in predicting dynamic responses. Recent research endeavors, notably those presented in [7], [8], and [9], have substantially advanced our understanding of non-uniform Rayleigh beams. These contributions have yielded valuable analytical solutions for dynamic responses, enabling engineers to capture the intricacies of real-world structures. By integrating non-uniformities into their analyses, engineers can garner a deeper insight into the dynamic behavior of structures, ultimately facilitating the design of safer, more efficient systems. Intensive damping in beams is a ubiquitous phenomenon in real-world structures, where energy dissipation occurs due to various factors such as friction, air resistance, and material viscosity. In bridges, for instance, damping helps mitigate the effects of wind and traffic-induced vibrations, ensuring structural stability. Similarly, in aircraft wings, damping plays a crucial role in reducing the impact of turbulence and aerodynamic forces. Although studies have investigated damping in uniform beams [10], [11] and [12], and some have considered non-uniform beams [13], [14], [15], [16] these works often neglect the dynamic response of damped and non-uniform beams subjected to harmonic moving loads on an exponentially decaying foundation. Notably, research by [17], and [18] has addressed the dynamic behavior of non-uniform beams, but with limited consideration of damping effects under harmonic moving loads and without accounting for the exponential decay of the foundation. This knowledge deficit highlights the need for a comprehensive analysis of damped and non-uniform beams under harmonic moving loads on an exponentially decaying foundation. The present work aims to address this shortcoming by providing an accurate and efficient method for analyzing the dynamic response of such beams, which is essential for accurately predicting the dynamic response of real-world structures.

2 Methodology

A fourth-order partial differential equation governs the dynamic behavior of the beam. Suppose that a harmonic moving load is applied to a non-uniform Rayleigh beam of length L. From time $t = 0$, the load moves along the beam at a constant velocity c. A fourth-order partial differential equation determined by [19] serves as the governing equation.

$$\frac{\partial^2}{\partial y^2}\left[EI(y)\frac{\partial^2 Q^*(y,t)}{\partial y^2}\right] - N\frac{\partial^2 Q^*(y,t)}{\partial y^2} + \mu(y)\frac{\partial^2 Q^*(y,t)}{\partial t^2} - \mu(y)r^0\frac{\partial^4 Q^*(y,t)}{\partial y^2 \partial t^2} + D(y)\frac{\partial Q^*(y,t)}{\partial t} + P(y)Q(y,t) = F(y,t) \tag{1}$$

where $EI(y)$ is the variable flexural rigidity of the structure, t is the time co-ordinate, y is the spatial co-ordinate, $Q^*(y,t)$ is the beam deflection, $\mu(y)$ is the variable mass per unit length of non-uniform beam, N is the axial force, r^0 is the rotatory inertia factor, $P(y)$ is the exponetial decaying foundation, $F(y,t)$ is the tranvelling load. $D(y)$ is the material variable damping intensity

The non-uniform properties of the beam can be effectively represented using power functions, as demonstrated [20], to approximate the real non-uniformity of the beam, the β and n parameters are utilized, as

$$\begin{aligned} I(y) &= I_0(1+\beta y)^{n+2} \\ \mu(y) &= \mu_0(1+\beta y)^n \\ D(y) &= D_o(1+\beta y)^n \end{aligned} \tag{2}$$

where the constant damping intensity is D_0, the constant mass per unit length of the beam is μ_0, and the constant moment of inertia is I_0.

For the sake of generality, it is assumed that the beam is in a state of equilibrium at the beginning, with neither displacement nor velocity. Hence, the initial conditions are:

$$Q^*(y,0) = 0 \tag{3}$$

and

$$\frac{\partial Q^*(y,0)}{\partial t} = 0 \tag{4}$$

We model the elastic foundation using an exponentially decaying function, $P(y)$ as introduced by [21], which takes the form:

$$P(y) = P_0 e^{-\alpha y} \tag{5}$$

where α is a constant and P_0 is the elastic foundation constant

Considering the impact of the harmonic load on the beam's response, the load $F(y,t)$ can be represented as:

$$F(y,t) = F_f(y,t)\left[1 - \frac{d^2}{dt^2}[\cdot]\left[\frac{Q^*(y,t)}{g}\right]\right] \tag{6}$$

While the harmonic force $F_f(y,t)$ acting on this engineering structure is given as

$$F_f(y,t) = Mg\cos\omega t H(y-ct) \tag{7}$$

The time t domain of interest is when the mass is on the beam, where the load is modeled as a distributed mass M.

$$0 \le ct \le L \tag{8}$$

Where $H(y-ct)$ is the heaviside function which is defined as

$$H(y-ct) = \begin{cases} 0, & y < ct; \\ 1, & y \ge ct. \end{cases} \tag{9}$$

with the properties

i

$$\frac{d}{dy}\big(H(y-ct)\big) = \delta(y-ct) \tag{10}$$

ii

$$f(y)H(y-ct) = \begin{cases} 0, & y < ct; \\ f(y), & y > ct. \end{cases} \tag{11}$$

where the Dirac delta function is represented by $\delta(y-ct)$ is a common engineering function used to measure "of" or "on" functions, which are frequently used in engineering applications.
The operator $\frac{d^2}{dt^2}[\cdot]$ used in (6) is defined as

$$\frac{d^2}{dt^2}[\cdot] = \frac{\partial^2}{\partial t^2} + 2c\frac{\partial^2}{\partial y \partial t} + c^2\frac{\partial^2}{\partial y^2} \tag{12}$$

Substituting equations (2), (5), (6), (7)and (12) into equation (1) and taking n = 1 for simplicity yields.

$$\begin{aligned} &\frac{\partial^2}{\partial y^2}\left[EI_0(1+\beta y)^3\frac{\partial^2 Q^*(y,t)}{\partial y^2}\right] - N\frac{\partial^2 Q^*(y,t)}{\partial y^2} + \mu_0(1+\beta y)\frac{\partial^2 Q^*(y,t)}{\partial t^2} - \mu_0(1+\beta y)r^0\frac{\partial^4 Q^*(y,t)}{\partial y^2 \partial t^2} \\ &+ D_o(1+\beta y)\frac{\partial Q^*(y,t)}{\partial t} + P_0 e^{-\alpha y}Q^*(y,t) + M\cos\omega t H(y-ct)\left[\frac{\partial^2}{\partial t^2} + 2c\frac{\partial^2}{\partial y \partial t} + c^2\frac{\partial^2}{\partial y^2}\right]Q^*(y,t) \\ &= Mg\cos\omega t H(y-ct) \end{aligned} \tag{13}$$

2.1 Approximate Analytical Solution

The beam problem presented in equation (13) will be addressed using Galerkin's method, a robust and versatile technique commonly employed to solve mechanical vibration problems. Notably, the Galerkin approach offers distinct advantages over traditional Finite Element Methods (FEM), including improved accuracy and computational efficiency, particularly for problems with complex geometries and boundary conditions. By leveraging these benefits, the Galerkin method provides a more rigorous and efficient solution, capturing the underlying physics of the problem with fewer degrees of freedom. The equation of motion for a beam element is symbolically represented by:

$$\Gamma(Q^*(y,t)) - F(y,t) = 0 \tag{14}$$

where Γ is the differential operator that has variable coefficients. The solution form for equation (13) is given by:

$$Q_j^*(y,t) = \sum_{j=1}^{\infty} W_j^*(t)Z_j^*(y) \tag{15}$$

where $W_j^*(t)$ are coordinates in modal space and $Z_j^*(y)$ are the normal modes of free vibration written as

$$Z_j^*(y) = \sin\frac{a_j y}{L} + A_j \cos\frac{a_j y}{L} + B_j \sinh\frac{a_j y}{L} + C_j \cosh\frac{a_j y}{L} \tag{16}$$

where the beam vibration's amplitude and space are defined by the constants A_j, B_j, and C_j. Their values are determined by the structure's related boundary condition. Using equation (15) into equation (13), we obtain:

$$\begin{aligned}
&EI_0\Bigg[\Big(1+3\beta y+3\beta^2y^2+\beta^3y^3\Big)\frac{\partial^4}{\partial y^4}\sum_{j=1}^{N}W_j^*(t)Z_j^*(y)+\Big(6\beta y+12\beta^2y+6\beta^3y^2\Big)\frac{\partial^3}{\partial y^3}\sum_{j=1}^{N}W_j^*(t)Z_j^*(y)\\
&+\Big(6\beta^2+6\beta^3y\Big)\frac{\partial^2}{\partial y^2}\sum_{j=1}^{N}W_j^*(t)Z_j^*(y)\Bigg]+\mu_0\Big(1+\beta y\Big)\frac{\partial^2}{\partial t^2}\sum_{j=1}^{N}W_j^*(t)Z_j^*(y)-N\frac{\partial^2}{\partial y^2}\sum_{j=1}^{N}W_j^*(t)Z_j^*(y)\\
&+D_o\Big(1+\beta y\Big)\frac{\partial}{\partial t}\sum_{j=1}^{N}W_j^*(t)Z_j^*(y)-\mu_0 r^0\Big(1+\beta y\Big)\frac{\partial^4}{\partial y^2t^2}\sum_{j=1}^{N}W_j^*(t)Z_j^*(y)+P_0e^{\alpha y}\sum_{j=1}^{N}W_j^*(t)Z_j^*(y)\\
&+M\cos\omega t H(y-ct)\Big[\frac{\partial^2}{\partial t^2}+2c\frac{\partial^2}{\partial y\partial t}+c^2\frac{\partial^2}{\partial y^2}\Big]\sum_{j=1}^{N}W_j^*(t)Z_j^*(y)-Mg\cos\omega t H(y-ct)=0
\end{aligned} \tag{17}$$

To determine $Q_j^*(t)$, the right-hand side of equation (17) must be orthogonal to the function $Z_k^*(y)$. So that

$$Z_k^*(y) = \sin\frac{a_k y}{L} + A_k \cos\frac{a_k y}{L} + B_k \sinh\frac{a_k y}{L} + C_k \cosh\frac{a_k y}{L} \tag{18}$$

The unknown constants A_j, B_j, C_j, A_k, B_k, C_k and the natural frequencies a_j, a_k in equation (16) and (18) are obtained by applying classical boundary conditions. Consequently, equation (17) becomes:

$$\begin{aligned}
&\sum_{j=0}^{N}\Bigg\{\frac{EI_0}{\mu_0}\Bigg(\int_0^L Z_j^{*iv}(y)Z_k^*(y)dy+3\beta\int_0^L yZ_j^{*iv}(y)Z_k^*(y)dy+3\beta^2\int_0^L y^2Z_j^{*iv}(y)Z_k^*(y)dy\\
&+\beta^3\int_0^L y^3Z_j^{*iv}(y)Z_k^*(y)dy+6\beta\int_0^L Z_j^{*'''}(y)Z_k^*(y)dy+12\beta^2\int_0^L yZ_j^{*'''}(y)Z_k^*(y)dy\\
&+6\beta^3\int_0^L y^2Z_j^{*'''}(y)Z_k^*(y)dy+6\beta^2\int_0^L Z_j^{*''}(y)Z_k^*(y)dy+6\beta^3\int_0^L yZ_j^{*''}(y)Z_k^*(y)dy\Bigg)W_j^*(t)\\
&+\Bigg(\int_0^L Z_j^*(y)Z_k^*(y)dy+\beta\int_0^L yZ_j^*(y)Z_k^*(y)dy\Bigg)\ddot{W}^*{}_j(t)-\frac{N}{\mu_0}\int_0^L Z_j^{*''}(y)Z_k^*(y)dyW_j^*(t)\\
&\frac{D_o}{\mu_0}\Bigg(\int_0^L Z_j^*(y)Z_k^*(y)dy+\beta\int_0^L yZ_j^*(y)Z_k^*(y)dy\Bigg)\dot{W}^*{}_j(t)+r^0\Bigg(\int_0^L Z_j^{*''}(y)Z_k^*(y)dy\\
&+\beta\int_0^L yZ_j^{*''}Z_k^*(y)dy\Bigg)\ddot{W}^*{}_j(t)+\frac{P_0}{\mu_0}\int_0^L e^{-\alpha y}Z_j^*(y)Z_k^*(y)dy+\frac{M\cos\omega t}{\mu_0 L}\Bigg(L\Bigg(\int_0^L H(y-ct)Z_j^*(y)Z_k^*(y)dy\Bigg)\ddot{W}^*{}_j(t)\\
&+2cL\Bigg(\int_0^L H(y-ct)Z_j^{*'}(y)Z_k^*(y)dy\Bigg)\ddot{W}^*{}_j(t)+c^2L\Bigg(\int_0^L H(y-ct)Z_j^{*''}(y)Z_k^*(y)dy\Bigg)W_j^*(t)\Bigg)\\
&-\frac{Mg\cos\omega t}{\mu_0}\int_0^L H(y-ct)Z_k^*(y)dy\Bigg\}=0
\end{aligned} \tag{19}$$

After simplification and arrangement of equation (19) one gets

$$\sum_{j=0}^{N}\Bigg\{\frac{EI_0}{\mu_0}\Bigg(A_1(j,k)+3\beta A_2(j,k)+3\beta^2A_3(j,k)+\beta^3A_4(j,k)+6\beta A_5(j,k)+12\beta^2A_6(j,k)$$
$$+6\beta^3A_7(j,k)+6\beta^2A_8(j,k)+6\beta^3A_9(j,k)\Bigg)W_j^*(t)+\Bigg(A_{10}(j,k)+\beta A_{11}(j,k)\Bigg)\ddot{W^*}_j(t)-\frac{N}{\mu_0}A_8(j,k)W_j^*(t)$$
$$+\frac{D_0}{\mu_0}\Bigg(A_{10}(j,k)+A_{11}(j,k)\Bigg)\dot{W^*}_j(t)+r^0\Bigg(A_8(j,k)+A_9(j,k)\Bigg)\ddot{W^*}_j(t)+\frac{P_0}{\mu_0}A_{12}(j,k)W_j^*(t)$$
$$+\xi_0\cos\omega t\Bigg(LA_{13}(j,k)\ddot{W^*}_j(t)+2cLA_{14}(j,k)\ddot{W^*}_j(t)+c^2LA_{15}(j,k)W_j^*(t)\Bigg)\Bigg\}=\frac{Mg\cos\omega t}{\mu_0}A_{16}(t) \tag{20}$$

where

$$A_1(j,k)=\int_0^L Z_j^{*iv}(y)Z_k^*(y)dy \qquad A_9(j,k)=\int_0^L yZ_j^{*''}(y)Z_k^*(y)dy$$
$$A_2(j,k)=\int_0^L yZ_j^{*iv}(y)Z_k^*(y)dy \qquad A_{10}(j,k)=\int_0^L Z_j^*(y)Z_k^*(y)dy$$
$$A_3(j,k)=\int_0^L y^2Z_j^{*iv}(y)Z_k^*(y)dy \qquad A_{11}(j,k)=\int_0^L yZ_j^*(y)Z_k^*(y)dy$$
$$A_4(j,k)=\int_0^L y^3Z_j^{*iv}(y)Z_k^*(y)dy \qquad A_{12}(j,k)=\int_0^L e^{-\alpha y}Z_j^*(y)Z_k^*(y)dy$$
$$A_5(j,k)=\int_0^L Z_j^{*'''}(y)Z_k^*(y)dy \qquad A_{13}(j,k)=\int_0^L H(y-ct)Z_j^*(y)Z_k^*(y)dy$$
$$A_6(j,k)=\int_0^L yZ_j^{*'''}(y)Z_k^*(y)dy \qquad A_{14}(j,k)=\int_0^L H(y-ct)Z_j^{*'}(y)Z_k^*(y)dy$$
$$A_7(j,k)=\int_0^L y^2Z_j^{*'''}(y)Z_k^*(y)dy \qquad A_{15}(j,k)=\int_0^L H(y-ct)Z_j^{*'''}(y)Z_k^*(y)dy$$
$$A_8(j,k)=\int_0^L Z_j^{*''}(y)Z_k^*(y)dy \qquad A_{16}(j,k)=\int_0^L H(y-ct)Z_k^*(y)dy \tag{21}$$

$\xi=\frac{M}{L\mu_0}$ is the inertia term.

In order to solve this equation, Using the Fourier series representation of the Heaviside unit step function, namely,

$$H(y-ct)=\frac{1}{4}+\frac{1}{\pi}\sum_0^\infty\frac{\sin(2n+1)\pi(y-ct)}{(2n+1)}, \qquad 0<y<L \tag{22}$$

Substituting equation (16), (18) and (22) into (20) after some simplification and rearrangement, one obtains.

$$
\begin{aligned}
&(H_1+H_2+H_6)W_j^*(t)+H_3\dot{W^*}_j(t)+(H_4+H_5)\ddot{W^*}_j(t)+\xi\cos\omega t\Bigg\{L\Bigg(\frac{1}{4}B_1(j,k)\\
&+\frac{1}{\pi}\sum_0^\infty\frac{\cos(2n+1)\pi ct}{(2n+1)}B_{1a}(n,j,k)-\frac{1}{\pi}\sum_0^\infty\frac{\sin(2n+1)\pi ct}{(2n+1)}B_{1b}(n,j,k)\Bigg)\ddot{W^*}_j(t)\\
&+2Lc\Bigg(\frac{1}{4}B_2(j,k)+\frac{1}{\pi}\sum_0^\infty\frac{\cos(2n+1)\pi ct}{(2n+1)}B_{2a}(n,j,k)-\frac{1}{\pi}\sum_0^\infty\frac{\sin(2n+1)\pi ct}{(2n+1)}B_{2b}(n,j,k)\Bigg)\dot{W^*}_j(t)\\
&+\Bigg(Lc^2\Bigg(\frac{1}{4}B_3(j,k)+\frac{1}{\pi}\sum_0^\infty\frac{\cos(2n+1)\pi ct}{(2n+1)}B_{3a}(n,j,k)-\frac{1}{\pi}\sum_0^\infty\frac{\sin(2n+1)\pi ct}{(2n+1)}B_{3b}(n,j,k)\Bigg)W_j^*\Bigg\}\\
&=\frac{LMg\cos\omega t}{a_k\mu_0}\Bigg(\theta_{JC}+\cos\gamma t-A_k\sin\gamma t-B_k\cosh\gamma t-C_k\sinh\gamma t\Bigg)
\end{aligned}
\tag{23}
$$

where

$$
\gamma=\frac{k\pi c}{L},\quad \theta_{JC}=-\cos a_k+A_k\sin a_k+B_k\cosh a_k+C_k\sinh a_k
$$

$$
\begin{aligned}
H_1&=\frac{EI_0}{\mu_0}\Bigg(A_1(j,k)+3\beta A_2(j,k)+3\beta^2A_3(j,k)+\beta^3A_4(j,k)+6\beta A_5(j,k)+12\beta^2A_6(j,k)\\
&+6\beta^3A_7(j,k)+6\beta^2A_8(j,k)+6\beta^3A_9(j,k)\Bigg),\quad H_2=\frac{N}{\mu_0}A_8(j,k),\quad H_3=\frac{D_o}{\mu_0}\Bigg(A_{10}(j,k)+A_{11}(j,k)\Bigg),\\
H_4&=\Bigg(A_{10}(j,k)+\beta A_{11}(j,k)\Bigg),\quad H_5=r^0\Bigg(A_8(j,k)+A_9(j,k)\Bigg)\ \text{ and }\ H_6=\frac{P_0}{\mu_0}A_{12}(j,k)
\end{aligned}
$$

$$
\begin{aligned}
B_{1a}(j,k)&=A_{10}(j,k)\\
B_{1b}(n,j,k)&=\int_0^L sin(2n+1)\pi yZ_j^*(y)Z_k^*(y)dy\\
B_{1c}(n,j,k)&=\int_0^L cos(2n+1)\pi yZ^*j(y)Z_k^*(y)dy\\
B_{2a}(j,k)&=\int_0^L Z_j^{*'}(y)Z_k^*(y)dy\\
B_{2b}(n,j,k)&=\int_0^L sin(2n+1)\pi yZ_j^{*'}(y)Z_k^*(y)dy\\
B_{2c}(n,j,k)&=\int_0^L cos(2n+1)\pi yZ_j^{*'}(y)Z_k^*(y)dy\\
B_{3a}(j,k)&=A_8(j,k)\\
B_{3b}(n,j,k)&=\int_0^L sin(2n+1)\pi yZ_j^{*''}(y)Z_k^*(y)dy\\
B_{3c}(n,j,k)&=\int_0^L cos(2n+1)\pi yZ_j^{*''}(y)Z_k^*(y)dy
\end{aligned}
\tag{24}
$$

Equation (23) governs the non-uniform damped Rayleigh beam on an exponentially decaying foundation subjected to a harmonic moving load. Two special cases are now discussed.

2.2 Non-uniform Damped Rayleigh Beam Traversed by Moving Force

By neglecting the inertia terms, setting $\xi = 0$, a simplified model of the differential equation governing the dynamic response is derived. As a result, Equation (23) simplifies to:

$$\ddot{W^*}_j(t) + \sigma_1 \dot{W^*}_j(t) + \sigma_2 W_j^*(t) = A_J \cos\omega t \Big(\theta_{JC} + \cos\gamma t - A_k \sin\gamma t - B_k \cosh\gamma t - C_k \sinh\gamma t \Big) \tag{25}$$

where

$$\sigma_1 = \frac{H_3}{H_4 + H_5}, \quad \sigma_2 = \frac{H_1 + H_2 + H_6}{H_4 + H_5}, \quad \text{and} \quad A_J = \frac{MgL}{k\pi\mu_0 A_3(j,k)(H_4 + H_5)} \tag{26}$$

Equation (25) is a second-order ordinary differential equation, and it can be solved using the Laplace transform method. The Laplace transform is defined as:

$$L\{f(t)\} = \int_0^\infty f(t) e^{-St} \tag{27}$$

In conjunction with the initial conditions define in equation (3)and (4), yields the following algebraic equation

$$\begin{aligned} \Big(S^2 + S\sigma_1 + \sigma_2\Big) W_j^*(S) = \frac{A_J}{2} \Bigg(2\theta_{JC} \frac{S}{S^2+\omega^2} + \frac{S}{S^2+\Theta_1^2} + \frac{S}{S^2+\Theta_2^2} - A_k \Big(\frac{\Theta_1}{S^2+\Theta_1^2} + \frac{\Theta_2}{S^2+\Theta_2^2} \Big) \\ - B_k \Big(\frac{S-\gamma}{(S-\gamma)^2+\omega^2} + \frac{S+\gamma}{(S+\gamma)^2+\omega^2} \Big) - C_k \Big(\frac{S-\gamma}{(S-\gamma)^2+\omega^2} - \frac{S+\gamma}{(S+\gamma)^2+\omega^2} \Big) \Bigg) \end{aligned} \tag{28}$$

where $\Theta_1 = \gamma + \omega \quad$ and $\quad \Theta_2 = \gamma - \omega$.

Simplifying equation (32) further yields:

$$\begin{aligned} W_j^*(S) = \frac{A_J}{2(\rho_1 - \rho_2)} \Bigg\{ \Bigg(2\theta_{JC} \frac{S}{S^2+\omega^2} + \frac{S}{S^2+\Theta_1^2} + \frac{S}{S^2+\Theta_2^2} - A_k \Big(\frac{\Theta_1}{S^2+\Theta_1^2} + \frac{\Theta_2}{S^2+\Theta_2^2} \Big) \\ - B_k \Big(\frac{S-\gamma}{(S-\gamma)^2+\omega^2} + \frac{S+\gamma}{(S+\gamma)^2+\omega^2} \Big) - C_k \Big(\frac{S-\gamma}{(S-\gamma)^2+\omega^2} - \frac{S+\gamma}{(S+\gamma)^2+\omega^2} \Big) \Bigg\} \frac{1}{S-\rho_1} \\ - \Bigg\{ \Bigg(2\theta_{JC} \frac{S}{S^2+\omega^2} + \frac{S}{S^2+\Theta_1^2} + \frac{S}{S^2+\Theta_2^2} - A_k \Big(\frac{\Theta_1}{S^2+\Theta_1^2} + \frac{\Theta_2}{S^2+\Theta_2^2} \Big) \\ - B_k \Big(\frac{S-\gamma}{(S-\gamma)^2+\omega^2} + \frac{S+\gamma}{(S+\gamma)^2+\omega^2} \Big) - C_k \Big(\frac{S-\gamma}{(S-\gamma)^2+\omega^2} - \frac{S+\gamma}{(S+\gamma)^2+\omega^2} \Big) \Bigg\} \frac{1}{S-\rho_2} \end{aligned} \tag{29}$$

Where

$$\rho_1 = -\frac{\sigma_1}{2} + \frac{\sqrt{\sigma_1^2 - 4\sigma_2}}{2} \tag{30}$$

$$\rho_2 = -\frac{\sigma_1}{2} - \frac{\sqrt{\sigma_1^2 - 4\sigma_2}}{2} \tag{31}$$

To obtain the inverse transform of equation (29), we will utilize the following representation:

$$\begin{aligned} F_1(S) = \frac{1}{S-\rho_1}, \quad F_2(S) = \frac{1}{S-\rho_2} \\ G(S) = \Bigg(2\theta_{JC} \frac{S}{S^2+\omega^2} + \frac{S}{S^2+\Theta_1^2} + \frac{S}{S^2+\Theta_2^2} - A_k \Big(\frac{\Theta_1}{S^2+\Theta_1^2} + \frac{\Theta_2}{S^2+\Theta_2^2} \Big) \\ - B_k \Big(\frac{S-\gamma}{(S-\gamma)^2+\omega^2} + \frac{S+\gamma}{(S+\gamma)^2+\omega^2} \Big) - C_k \Big(\frac{S-\gamma}{(S-\gamma)^2+\omega^2} - \frac{S+\gamma}{(S+\gamma)^2+\omega^2} \Big) \end{aligned} \tag{32}$$

The convolution of F_i and G corresponds to the inverse Laplace transform of equation (29), given by:

$$F_i * G = \int_0^t F_i(t-u)G(u)du \qquad i = 1, 2 \tag{33}$$

Thus the Laplace inversion of equation (29) is given by:

$$W_j^*(t) = \frac{A_J}{2(\rho_1 - \rho_2)}\Bigg(2\theta_{JC}I_1 + I_2 + I_3 - A_K(I_4 + I_5) - B_k(I_6 + I_7) - C_k(I_6 - I_7) - 2\theta_{JC}I_8 - I_9 - I_{10}$$
$$+ A_k(I_{11} + I_{12}) + B_k(I_{13} + I_{14}) + C_k(I_{13} - I_{14})\Bigg) \tag{34}$$

where

$$I_1 = \int_0^t e^{\rho_1(t-u)}\cos\omega u du \qquad I_8 = \int_0^t e^{\rho_2(t-u)}\cos\omega u du$$
$$I_2 = \int_0^t e^{\rho_1(t-u)}\cos\Theta_1 u du \qquad I_9 = \int_0^t e^{\rho_2(t-u)}\cos\Theta_1 u du$$
$$I_3 = \int_0^t e^{\rho_1(t-u)}\cos\Theta_2 u du \qquad I_{10} = \int_0^t e^{\rho_2(t-u)}\cos\Theta_2 u du$$
$$I_4 = \int_0^t e^{\rho_1(t-u)}\sin\Theta_1 u du \qquad I_{11} = \int_0^t e^{\rho_2(t-u)}\sin\Theta_1 u du$$
$$I_5 = \int_0^t e^{\rho_1(t-u)}\sin\Theta_2 u du \qquad I_{12} = \int_0^t e^{\rho_2(t-u)}\sin\Theta_2 u du$$
$$I_6 = \int_0^t e^{\rho_1(t-u)}e^{\gamma u}\cos\omega u du \qquad I_{13} = \int_0^t e^{\rho_2(t-u)}e^{\gamma u}\cos\omega u du$$
$$I_7 = \int_0^t e^{\rho_1(t-u)}e^{-\gamma u}\cos\omega u du \qquad I_{14} = \int_0^t e^{\rho_2(t-u)}e^{-\gamma u}\cos\omega u du \tag{35}$$

It is simple to demonstrate that

$$I_1 = \frac{1}{\omega^2 + \rho_1^2}\Big(\omega\sin\omega t - \rho_1\cos\omega t + \rho_1 e^{\rho_1 t}\Big)$$
$$I_2 = \frac{1}{\Theta_1^2 + \rho_1^2}\Big(\Theta_1\sin\omega t - \rho_1\cos\Theta_1 t + \rho_1 e^{\rho_1 t}\Big)$$
$$I_3 = \frac{1}{\Theta_2^2 + \rho_1^2}\Big(\Theta_2\sin\omega t - \rho_1\cos\Theta_2 t + \rho_1 e^{\rho_1 t}\Big)$$
$$I_4 = \frac{1}{\Theta_1^2 + \rho_1^2}\Big(-\Theta_1\cos\omega t - \rho_1\sin\Theta_1 t + \Theta_1 e^{\rho_1 t}\Big)$$
$$I_5 = \frac{1}{\Theta_2^2 + \rho_1^2}\Big(-\Theta_2\cos\Theta t - \rho_1\sin\Theta_2 t + \Theta_2 e^{\rho_1 t}\Big)$$
$$I_6 = \frac{1}{\omega^2 + \Omega_1^2}\Big(\omega\sin\omega t e^{\gamma t} + \Omega_1\cos\omega t e^{\gamma t} - \Omega_1 e^{\rho_1 t}\Big)$$
$$I_7 = \frac{1}{\omega^2 + \Omega_2^2}\Big(\omega\sin\omega t e^{-\gamma t} - \Omega_2\cos\omega t e^{-\gamma t} + \Omega_2 e^{\rho_1 t)}\Big)$$
$$I_8 = \frac{1}{\omega^2 + \rho_2^2}\Big(\omega\sin\omega t - \rho_2\cos\omega t + \rho_1 e^{\rho_2 t}\Big)$$
$$I_9 = \frac{1}{\Theta_1^2 + \rho_2^2}\Big(\Theta_1\sin\omega t - \rho_2\cos\Theta_1 t + \rho_1 e^{\rho_2 t}\Big)$$

$$
\begin{aligned}
I_{10} &= \frac{1}{\Theta_2^2+\rho_2^2}\Big(\Theta_2\sin\omega t-\rho_2\cos\Theta_2 t+\rho_1 2e^{\rho_2 t}\Big)\\
I_{11} &= \frac{1}{\Theta_1^2+\rho_2^2}\Big(-\Theta_1\cos\omega t-\rho_2\sin\Theta_1 t+\Theta_1 e^{\rho_2 t}\Big)\\
I_{12} &= \frac{1}{\Theta_2^2+\rho_2^2}\Big(-\Theta_2\cos\Theta t-\rho_2\sin\Theta_2 t+\Theta_2 e^{\rho_2 t}\Big)\\
I_{13} &= \frac{1}{\omega^2+\Omega_3^2}\Big(\omega\sin\omega t e^{\gamma t}+\Omega_3\cos\omega t e^{\gamma t}-\Omega_3 e^{\rho_2 t}\Big)\\
I_{14} &= \frac{1}{\omega^2+\Omega_4^2}\Big(\omega\sin\omega t e^{-\gamma t}-\Omega_4\cos\omega t e^{-\gamma t}+\Omega_4 e^{\rho_2 t)}\Big)
\end{aligned}
\tag{36}
$$

where

$\Omega_1=\gamma-\rho_1$, $\Omega_2=\gamma+\rho_1$, $\Omega_3=\gamma-\rho_2$ and $\Omega_4=\gamma+\rho_2$

Substituting equation (36) into equation (34) and then using the result in equation (15) yields:

$$
\begin{aligned}
&Q_j^*(y,t)=\\
&\sum_{j=1}^{\infty}\Bigg\{\frac{A_J}{2(\rho_1-\rho_2)}\Bigg(2\theta_{JC}\frac{1}{\omega^2+\rho_1^2}\Big(\omega\sin\omega t-\rho_1\cos\omega t+\rho_1 e^{\rho_1 t}\Big)+\frac{1}{\Theta_1^2+\rho_1^2}\Big(\Theta_1\sin\omega t-\rho_1\cos\Theta_1 t+\rho_1 e^{\rho_1 t}\Big)\\
&+\frac{1}{\Theta_2^2+\rho_1^2}\Big(\Theta_2\sin\omega t-\rho_1\cos\Theta_2 t+\rho_1 e^{\rho_1 t}\Big)-A_K\Bigg(\frac{1}{\Theta_1^2+\rho_1^2}\Big(-\Theta_1\cos\omega t-\rho_1\sin\Theta_1 t+\Theta_1 e^{\rho_1 t}\Big)\\
&+\frac{1}{\Theta_2^2+\rho_1^2}\Big(-\Theta_2\cos\Theta t-\rho_1\sin\Theta_2 t+\Theta_2 e^{\rho_1 t}\Big)\Bigg)-B_k\Bigg(\frac{1}{\omega^2+\Omega_1^2}\Big(\omega\sin\omega t e^{\gamma t}+\Omega_1\cos\omega t e^{\gamma t}-\Omega_1 e^{\rho_1 t}\Big)\\
&+\frac{1}{\omega^2+\Omega_2^2}\Big(\omega\sin\omega t e^{-\gamma t}-\Omega_2\cos\omega t e^{-\gamma t}+\Omega_2 e^{\rho_1 t)}\Big)\Bigg)-C_k\Bigg(\frac{1}{\omega^2+\Omega_1^2}\Big(\omega\sin\omega t e^{\gamma t}+\Omega_1\cos\omega t e^{\gamma t}-\Omega_1 e^{\rho_1 t}\Big)\\
&-\frac{1}{\omega^2+\Omega_2^2}\Big(\omega\sin\omega t e^{-\gamma t}-\Omega_2\cos\omega t e^{-\gamma t}+\Omega_2 e^{\rho_1 t)}\Big)\Bigg)-2\theta_{JC}\frac{1}{\omega^2+\rho_2^2}\Big(\omega\sin\omega t-\rho_2\cos\omega t+\rho_1 e^{\rho_2 t}\Big)\\
&-\frac{1}{\Theta_1^2+\rho_2^2}\Big(\Theta_1\sin\omega t-\rho_2\cos\Theta_1 t+\rho_1 e^{\rho_2 t}\Big)-\frac{1}{\Theta_2^2+\rho_2^2}\Big(\Theta_2\sin\omega t-\rho_2\cos\Theta_2 t+\rho_1 2e^{\rho_2 t}\Big)\\
&+A_k\Bigg(\frac{1}{\Theta_1^2+\rho_2^2}\Big(-\Theta_1\cos\omega t-\rho_2\sin\Theta_1 t+\Theta_1 e^{\rho_2 t}\Big)+\frac{1}{\Theta_2^2+\rho_2^2}\Big(-\Theta_2\cos\Theta t-\rho_2\sin\Theta_2 t+\Theta_2 e^{\rho_2 t}\Big)\Bigg)\\
&+B_k\Bigg(\frac{1}{\omega^2+\Omega_3^2}\Big(\omega\sin\omega t e^{\gamma t}+\Omega_3\cos\omega t e^{\gamma t}-\Omega_3 e^{\rho_2 t}\Big)+\frac{1}{\omega^2+\Omega_4^2}\Big(\omega\sin\omega t e^{-\gamma t}-\Omega_4\cos\omega t e^{-\gamma t}+\Omega_4 e^{\rho_2 t)}\Big)\Bigg)\\
&+C_k\Bigg(\frac{1}{\omega^2+\Omega_3^2}\Big(\omega\sin\omega t e^{\gamma t}+\Omega_3\cos\omega t e^{\gamma t}-\Omega_3 e^{\rho_2 t}\Big)-\frac{1}{\omega^2+\Omega_4^2}\Big(\omega\sin\omega t e^{-\gamma t}-\Omega_4\cos\omega t e^{-\gamma t}+\Omega_4 e^{\rho_2 t)}\Big)\Bigg)\Bigg\}\\
&\times\Big(\sin\frac{a_j y}{L}+A_j\cos\frac{a_j y}{L}+B_j\sinh\frac{a_j y}{L}+C_j\cosh\frac{a_j y}{L}\Big)
\end{aligned}
\tag{37}
$$

Equation (37) is a mathematical representation of the transverse displacement response of a non-uniform damped Rayleigh beam supported by an exponentially decaying foundation, when subjected to harmonic moving forces.

2.2.1 Non-uniform Damped Rayleigh Beam Traversed by Moving Mass

When the inertia term is incorporated into the equation (23), the mass ratio becomes non-zero ($\xi\neq 0$), giving rise to the moving mass problem. In this case, a comprehensive solution to the equation is

required. Since an exact solution is impractical, equation (23) is simplified and rearranged into a more simple form.

$$(H_1+H_2+H_6)W_j^*(t)+H_3\dot{W}^*{}_j(t)+(H_4+H_5)\ddot{W}^*{}_j(t)+\xi_0\cos\omega t\Bigg(\triangle_1(n,j,k)\ddot{W}^*{}_j(t)$$
$$+\triangle_2(n,j,k)\dot{W}^*{}_j(t)+\triangle_3(n,j,k)W_j^*(t)\Bigg)=\frac{LMg\cos\omega t}{a_k\mu_0}\Bigg(\theta_{JC}+\cos\gamma t-A_k\sin\gamma t-B_k\cosh\gamma t-C_k\sinh\gamma t\Bigg) \tag{38}$$

where

$$\triangle_1(n,j,k)=L\Bigg(\frac{1}{4}B_1(j,k)+\frac{1}{\pi}\sum_0^\infty\frac{\cos(2n+1)\pi ct}{(2n+1)}B_{1a}(n,j,k)-\frac{1}{\pi}\sum_0^\infty\frac{\sin(2n+1)\pi ct}{(2n+1)}B_{1b}(n,j,k)\Bigg)$$
$$\triangle_2(n,j,k)=2Lc\Bigg(\frac{1}{4}B_2(j,k)+\frac{1}{\pi}\sum_0^\infty\frac{\cos(2n+1)\pi ct}{(2n+1)}B_{2a}(n,j,k)-\frac{1}{\pi}\sum_0^\infty\frac{\sin(2n+1)\pi ct}{(2n+1)}B_{2b}(n,j,k)\Bigg)$$
$$\triangle_3(n,j,k)=Lc^2\Bigg(\frac{1}{4}B_3(j,k)+\frac{1}{\pi}\sum_0^\infty\frac{\cos(2n+1)\pi ct}{(2n+1)}B_{3a}(n,j,k)-\frac{1}{\pi}\sum_0^\infty\frac{\sin(2n+1)\pi ct}{(2n+1)}B_{3b}(n,j,k)\Bigg) \tag{39}$$

Further simplification and arrangments of equation (38), one obtains

$$\ddot{W}_j^*(t)+C_{p1}\dot{W}_j^*(t)+C_{p2}W_j^*(t)=C_{p3} \tag{40}$$
$$C_{p1}=\frac{H_3+\xi\cos\omega t\triangle_2(n,j,k)}{(H_4+H_5)+\xi\cos\omega t\triangle_1(n,j,k)} \tag{41}$$
$$C_{p2}=\frac{(H_1+H_2+H_6)+\xi\cos\omega t\triangle_3(n,j,k)}{(H_4+H_5)+\xi\cos\omega t\triangle_1(n,j,k)} \tag{42}$$
$$C_{p3}=\frac{LMg\cos\omega t}{a_k\mu_0}\Bigg(\theta_{JC}+\cos\gamma t-A_k\sin\gamma t-B_k\cosh\gamma t-C_k\sinh\gamma t\Bigg)\times\frac{1}{(H_4+H_5)+\xi\cos\omega t\triangle_1(n,j,k)} \tag{43}$$

The fourth order Runge-Kutta scheme is used to solve equation (40), a solution to moving mass problem must be obtained as in equation (37).

3 Discussion of the Closed Form Solutions

Resonance conditions are critical, as the transverse displacement of the beam may increase indefinitely. Equation (52) reveals that for a non-uniformly damped Rayleigh beam on an exponentially decaying foundation, subjected to a harmonic moving load, unbounded growth of transverse displacement occurs when the resonance condition is satisfied, specifically when.

$$\rho_1=\rho_2,\quad \omega^2=-\rho_1^2,\quad \omega^2=-\rho_2^2,\quad \Theta_1^2=-\rho_1^2,\quad \Theta_2^2=-\rho_1^2,\quad \Theta_1^2=-\rho_2^2,\quad \Theta_2^2=-\rho_2^2,$$
$$\omega^2=-\Omega_1^2,\quad \omega^2=-\Omega_2^2,\quad \omega^2=-\Omega_3^2,\quad \text{or}\quad \omega^2=-\Omega_4^2 \tag{44}$$

The critical velocity at which this phenomenon occurs is determined by the following relation:

$$C_i=\left(\left(\frac{H_3}{H_4+H_5}\right)^2-4\frac{(H_1+H_2+H_6)}{H_4+H_5}\right)^{\frac{1}{2}} \tag{45}$$

4 Illustrative Examples

This section provides illustrative examples of classical boundary conditions, showcasing the practical application of the analytical framework established in this study.

4.1 Pinned-Pinned Boundary Condition

The pinned-pinned boundary condition, where the displacement at both ends of the beam is constrained to be zero but rotation is allowed, accurately models real-world scenarios where beams are supported by pins or hinges. This boundary condition is crucial for analyzing the static and dynamic behavior of beams under various loading conditions, providing valuable insights into their structural response. Specifically, the boundary conditions are

At $y = 0$ (left end): $Q^*(0,t) = 0$ (no displacement) and $\frac{\partial^2}{\partial y^2}Q^*(0,t) =$ (no moment)

At $y = L$ (right end): $Q^*(L,t) = 0$ (no displacement) and $\frac{\partial^2}{\partial y^2}Q^*(L,t) =$ (no moment)

and, hence for the normal modes;

$$Z_j^*(0,t) = Z_j^*(L,t) = 0, \quad \frac{\partial^2}{\partial y^2}Z_j^*(0,t) = \frac{\partial^2}{\partial y^2}Z_j^*(L,t) = 0 \tag{46}$$

This implies that;

$$Z_k^*(0,t) = Z_k^*(L,t) = 0, \quad \frac{\partial^2}{\partial y^2}Z_k^*(0,t) = \frac{\partial^2}{\partial y^2}Z_k^*(L,t) = 0 \tag{47}$$

Applying equation (46) and (47) to equation (25) yields

$$A_j = B_j = C_j = 0, \quad a_j = j\pi \quad \text{and} \quad a_k = k\pi \tag{48}$$

Then, by substituting these coefficients into equations (37) and (43), the displacement responses of a pined-pined non-uniform Rayleigh beam subjected to moving distributed forces and masses are obtained.

4.2 Fixed-Fixed Boundary Condition

The fixed-fixed boundary condition, where the displacement and rotation at both ends of the beam are constrained to be zero, accurately models real-world scenarios where beams are rigidly attached to supports. This boundary condition is essential for predicting the dynamic behavior of beams under various loading conditions, ensuring accurate results in structural analysis. For a beam with fixed-fixed ends, deflection and slope are zero at the boundaries. Specifically,the boundary conditions are:

At $y = 0$ (left end): $Q^*(0,t) = 0$ (no displacement) and $\frac{\partial}{\partial y}Q^*(0,t) =$ (no rotation)

At $y = L$ (right end): $Q^*(L,t) = 0$ (no displacement) and $\frac{\partial}{\partial y}Q^*(L,t) =$ (no rotation)

and, hence for the normal modes;

$$Z_j^*(0,t) = Z_j^*(L,t) = 0, \quad \frac{\partial}{\partial y}Z_j^*(0,t) = \frac{\partial}{\partial y}Z_j^*(L,t) = 0 \tag{49}$$

This implies that;

$$Z_k^*(0,t) = Z_k^*(L,t) = 0, \quad \frac{\partial}{\partial y}Z_k^*(0,t) = \frac{\partial}{\partial y}Z_k^*(L,t) = 0 \tag{50}$$

Applying equation (49) to equation (16) yields

$$\Rightarrow A_j = \frac{\sinh a_j - \sin a_j}{\cos a_j - A_j \cosh a_j} = \frac{\cos a_j - A_j \cosh a_j}{\sin a_j + \sinh a_j} = -C_j$$
$$B_j = -1 \tag{51}$$

The frequency equation become

$$\Rightarrow \quad \cos a_j \cosh a_j = 1 \tag{52}$$

The coefficients A_k, B_k, and C_k can be easily derived by substituting k for j in equations (51) and (52). Then, by substituting these coefficients into equations (37) and (43), the displacement responses of a fixed-fixed non-uniform Rayleigh beam subjected to moving distributed forces and masses are obtained.

4.3 Fixed-Free Boundary Condition (The Cantilever)

The fixed-free boundary condition, where one end of the beam is rigidly fixed and the other end is free to move and rotate, simulates real-world scenarios such as cantilever beams. This boundary condition is crucial for analyzing the dynamic behavior of beams with one end constrained and the other end subjected to external loads or environmental factors. According, the boundary condition:

At y = 0 (left end): $Q^*(0,t) = 0$ (no displacement) and $\frac{\partial}{\partial y}Q^*(0,t) = 0$ (no rotation)

At y = L (right end): $\frac{\partial^2}{\partial y^2}Q^*(L,t) = 0$ (no moment) and $\frac{\partial^3}{\partial y^3}Q^*(L,t) = 0$ (no shear force)

$$Q^*(0,t) = \frac{\partial}{\partial y}Q^*(0,t) = 0 \;\; and \;\; \frac{\partial^2}{\partial y^2}Q^*(L,t) = \frac{\partial^3}{\partial y^3}Q^*(L,t) = 0 \tag{53}$$

and, hence for the normal modes;

$$Z_j^*(0) = \frac{\partial}{\partial y}Z_j^*(0) = 0 \;\; and \;\; \frac{\partial^2}{\partial y^2}Z_j^*(L) = \frac{\partial^3}{\partial y^3}Z_j^*(L) = 0 \tag{54}$$

This implies that,

$$Z_k^*(0) = \frac{\partial}{\partial x}Z_k^*(0) = 0 \;\; and \;\; \frac{\partial^2}{\partial x^2}Z_k^*(L) = \frac{\partial^3}{\partial x^3}Z_k^*(L) = 0 \tag{55}$$

Substituting equation (46) into equation (26) yields

$$\Rightarrow A_k = -\frac{\sin a_k + \sinh a_k}{\cos a_k + \cosh a_k} = \frac{\cosh a_k + \cos a_k}{\sin a_k - \sinh a_k} = -C_k$$

$$C_k = -1 \tag{56}$$

And the frequency equation for both end conditions is

$$\cos a_k \cosh a_k = -1 \tag{57}$$

The coefficients A_j, B_j, and C_j can be easily derived by substituting j for k in equations (56) and (57). Then, by substituting these coefficients into equations (37) and (43), the displacement responses of a fixed-free non-uniform Rayleigh beam subjected to moving distributed forces and masses are obtained.

5 Numerical Results and Discussions

A numerical investigation was undertaken to validate the preceding analysis, focusing on a non-uniform Rayleigh beam with specified parameters: length $L = 100m$, load velocity $v = 8.128m/s$, elasticity E of $3.9012 \times 10^9 N/m^2$, a moment of inertia I of $2.87698 \times 10^{-3} kg/m^2$, and mass ratio $\xi = 0.5$. To facilitate a comprehensive analysis, the beam's response to the harmonic moving load will be examined using the established parameters. The investigation will encompass a broad range of foundation moduli, from $0N/m^3$ to $400000N/m^3$, and axial force values spanning $0N$ and $2.0 \times 10^8 N$.

Figures 1-12 illustrate the dynamic deflections of a pinned-pinned non-uniform damped Rayleigh beam system under harmonic moving forces and masses. The effects of various parameters, including speed c, span length L, mass ratio ξ, damping coefficient D_o, rotatory inertia r^0, and axial force N, on the beam's response amplitude are examined. Figure 1 shows the dynamic deflections of the beam under harmonic moving forces with $N = 3000000N$, $r^0 = 2.5$, and varying c values. Increasing c values lead to an increase in the response amplitude. A similar trend is observed in Figure 2 for a harmonic moving mass. Figures 3 and 4 illustrate the dynamic deflections of the beam under harmonic moving forces and masses, respectively, with $N = 3000000N$, $r^0 = 2.5$, and varying L values. The response amplitude decreases as L increases. Figures 5 and 6 show the dynamic deflections of the beam under harmonic moving forces and masses, respectively, with $N = 3000000N$, $r^0 = 2.5$, and varying ξ values. The response amplitude increases as ξ increases. Figures 7 and 8 illustrate the dynamic deflections of the beam under harmonic moving forces and masses, respectively, with $N = 3000000N$, $r^0 = 2.5$, and varying D_o values. Increasing D_o values lead to a decrease in the response amplitude. Figures 9 and 10 show the dynamic deflections of the beam under harmonic moving forces and masses, respectively, with $N = 3000000N$, $D_o = 1500$, and varying r^0 values. The response amplitude decreases as r^0 increases. Figures 11 and 12 illustrate the dynamic deflections of the beam under harmonic

moving forces and masses, respectively, with $\xi = 2.5$, $D_o = 1500$, and varying N values. The response amplitude decreases as N increases. Figures 13-24 illustrate the dynamic deflections of a fixed-fixed non-uniform damped Rayleigh beam system under harmonic moving forces and masses. The effects of various parameters, including speed c, span length L, mass ratio ξ, damping coefficient D_o, rotatory inertia r^0, and axial force N, on the beam's response amplitude are examined.

Figure 13 shows the dynamic deflections of the beam under harmonic moving forces with $N = 3000000N$, $r^0 = 2.5$, and varying c values. Increasing c values lead to an increase in the response amplitude. A similar trend is observed in Figure 14 for a harmonic moving mass. Figures 15 and 16 illustrate the dynamic deflections of the beam under harmonic moving forces and masses, respectively, with $N = 3000000N$, $r^0 = 2.5$, and varying L values. The response amplitude decreases as L increases. Figures 17 and 18 show the dynamic deflections of the beam under harmonic moving forces and masses, respectively, with $N = 3000000N$, $r^0 = 2.5$, and varying ξ values. The response amplitude increases as ξ increases. Figures 19 and 20 illustrate the dynamic deflections of the beam under harmonic moving forces and masses, respectively, with $N = 3000000N$, $r^0 = 2.5$, and varying D_o values. Increasing D_o values lead to a decrease in the response amplitude. Figures 21 and 22 show the dynamic deflections of the beam under harmonic moving forces and masses, respectively, with $N = 3000000N$, $D_o = 1500$, and varying r^0 values. The response amplitude decreases as r^0 increases. Figures 23 and 24 illustrate the dynamic deflections of the beam under harmonic moving forces and masses, respectively, with $\xi = 2.5$, $D_o = 1500$, and varying N values. The response amplitude decreases as N increases. Figures 25-36 illustrate the dynamic deflections of a fixed-free non-uniform damped Rayleigh beam system under harmonic moving forces and masses. The effects of various parameters, including speed c, span length L, mass ratio ξ, damping coefficient D_o, rotatory inertia r^0, and axial force N, on the beam's response amplitude are examined. Figure 25 shows the dynamic deflections of the beam under harmonic moving forces with $N = 3000000N$, $r^0 = 2.5$, and varying c values. Increasing c values lead to an increase in the response amplitude. A similar trend is observed in Figure 26 for a harmonic moving mass. Figures 27 and 28 illustrate the dynamic deflections of the beam under harmonic moving forces and masses, respectively, with $N = 3000000N$, $r^0 = 2.5$, and varying L values. The response amplitude decreases as L increases. Figures 29 and 30 show the dynamic deflections of the beam under harmonic moving forces and masses, respectively, with $N = 3000000N$, $r^0 = 2.5$, and varying ξ values. The response amplitude increases as ξ increases. Figures 31 and 32 illustrate the dynamic deflections of the beam under harmonic moving forces and masses, respectively, with $N = 3000000N$, $r^0 = 2.5$, and varying D_o values. Increasing D_o values lead to a decrease in the response amplitude. Figures 33 and 34 show the dynamic deflections of the beam under harmonic moving forces and masses, respectively, with $N = 3000000N$, $D_o = 1500$, and varying r^0 values. The response amplitude decreases as r^0 increases.

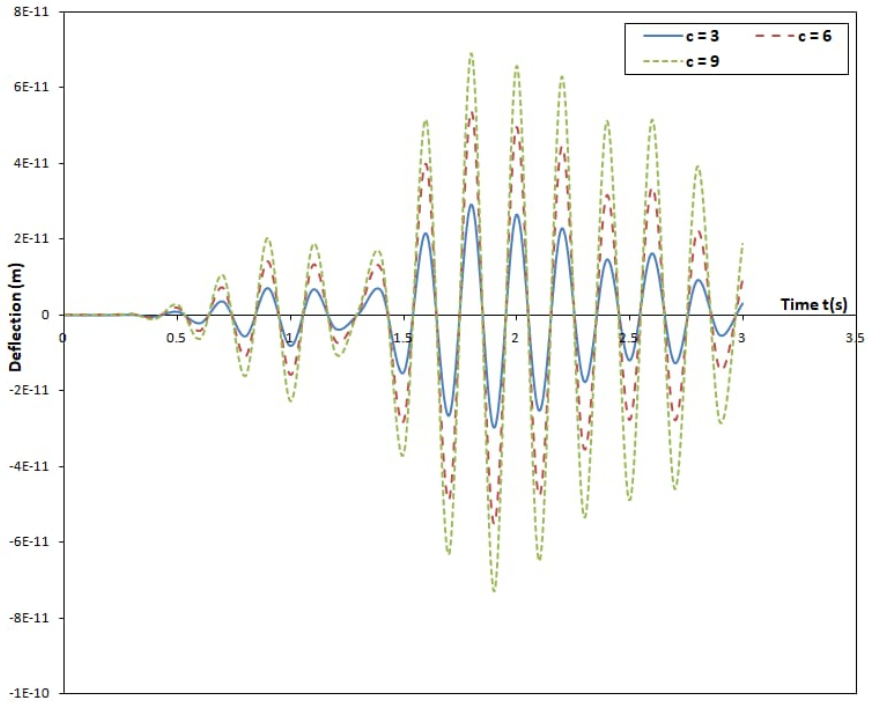

Figure 1:

The deflection profile of the moving force system's pinned-pinned non-uniform damped Rayleigh beam under the influence of a harmonic moving load for different speed values

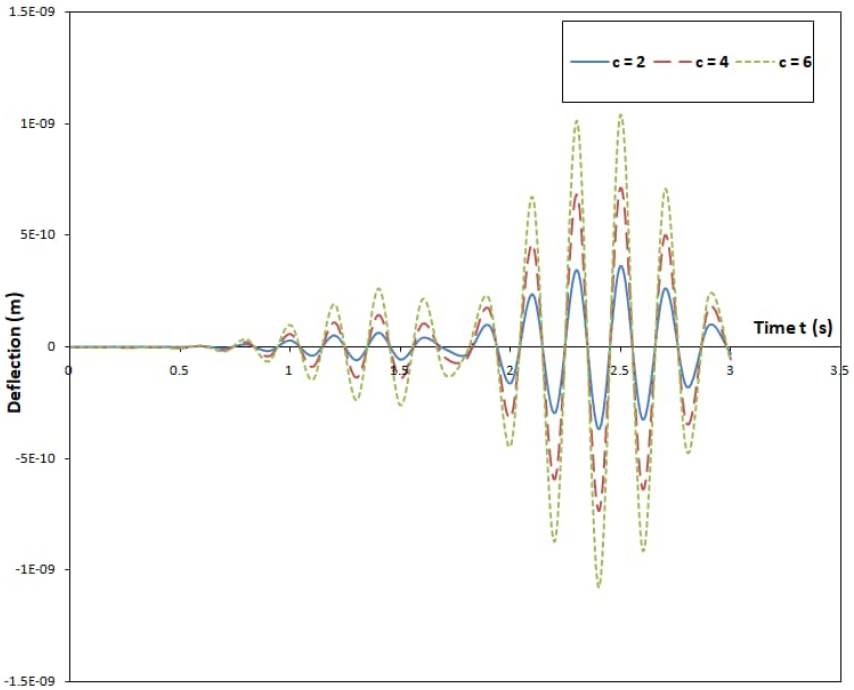

Figure 2:

The deflection profile of the moving mass system's pinned-pinned non-uniform damped Rayleigh beam under the influence of a harmonic moving load for different speed values

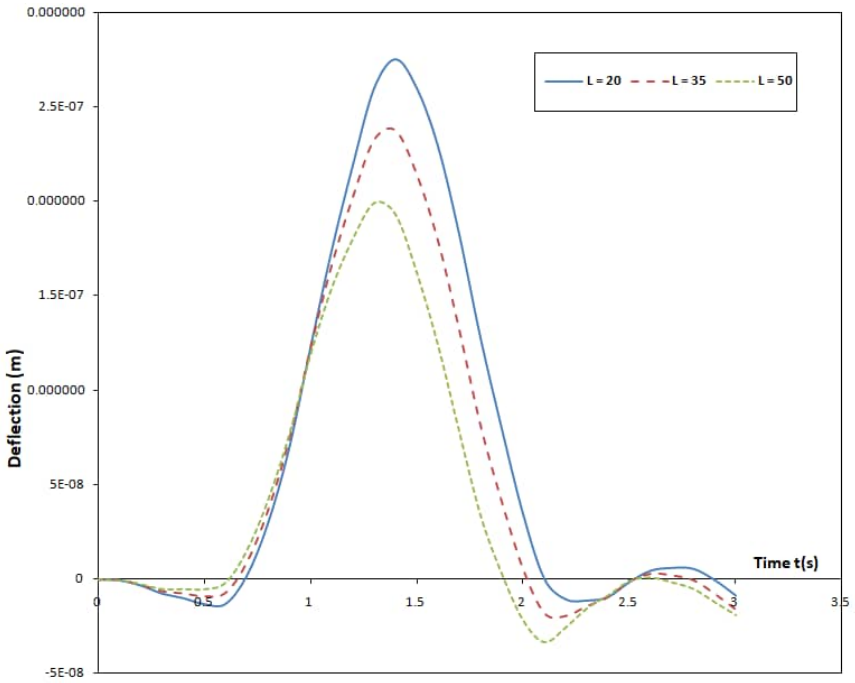

Figure 3:

The deflection profile of the moving force system's pinned-pinned non-uniform damped Rayleigh beam under the influence of a harmonic moving load for different Lenght values

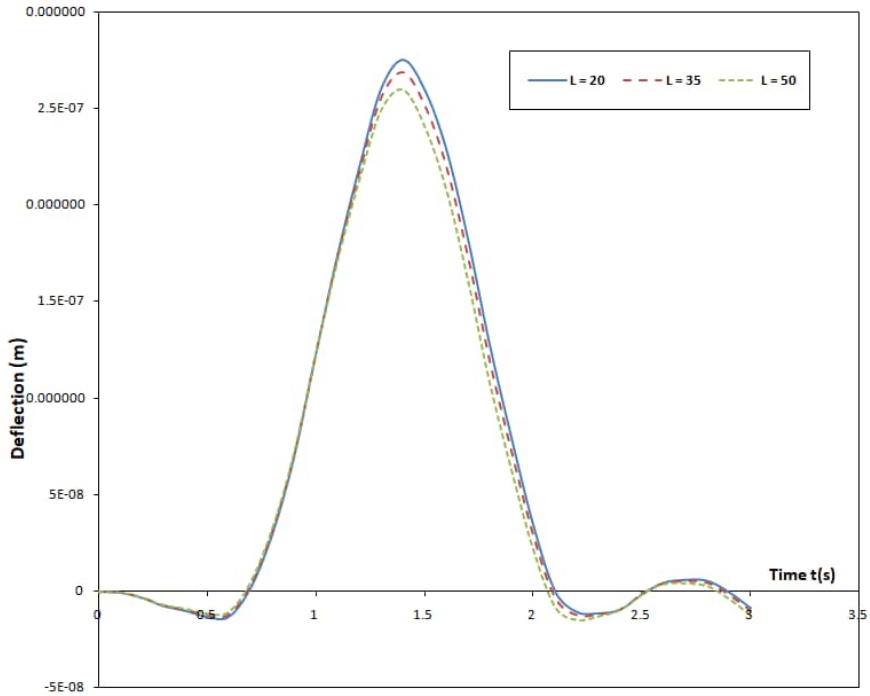

Figure 4:

The deflection profile of the moving mass system's pinned-pinned non-uniform damped Rayleigh beam under the influence of a harmonic moving load for different Lenght values

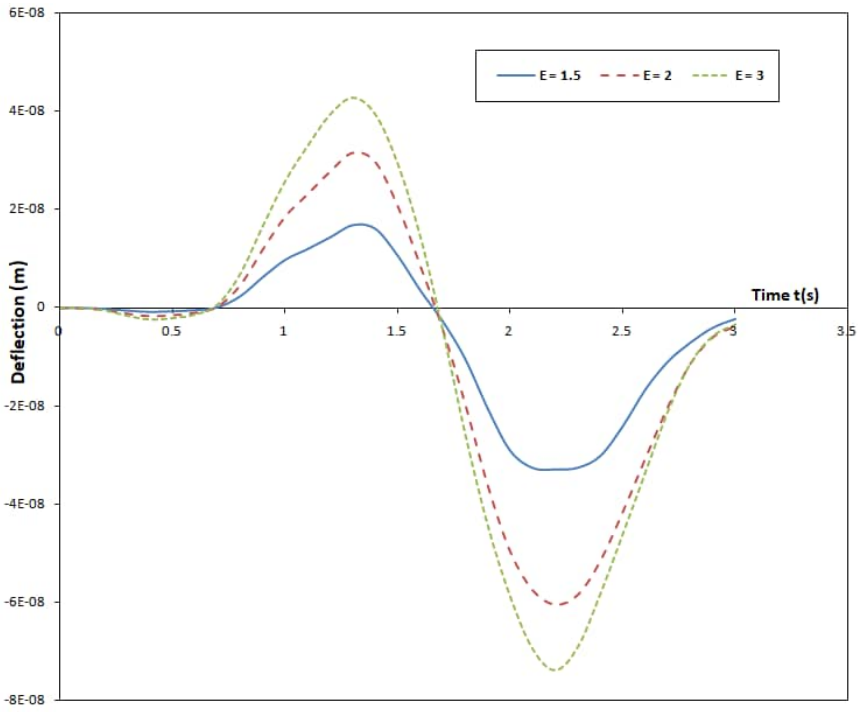

Figure 5:

The deflection profile of the moving force system's pinned-pinned non-uniform damped Rayleigh beam under the influence of a harmonic moving load for different mass ratio values

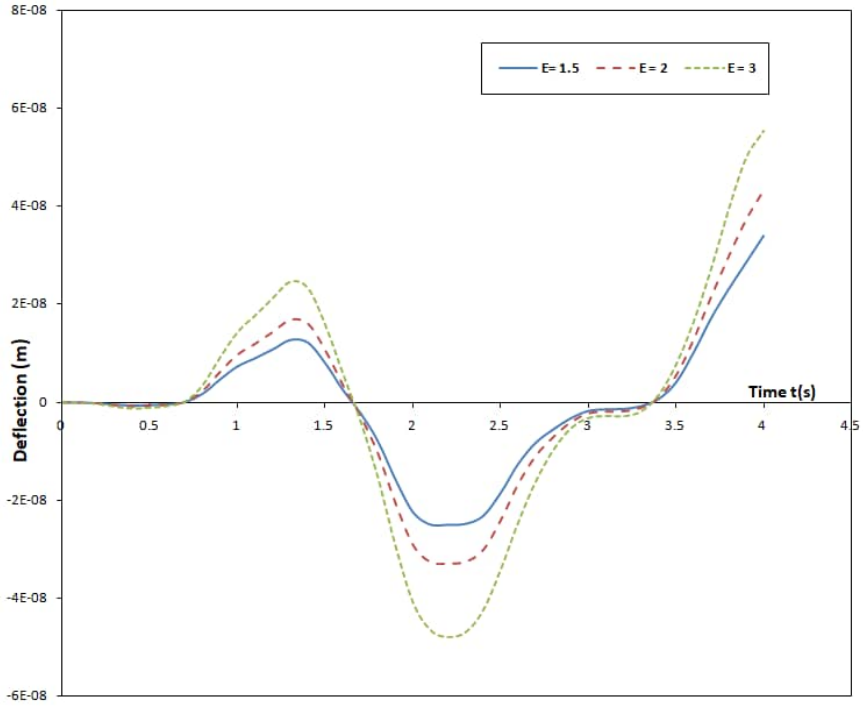

Figure 6:

The deflection profile of the moving mass system's pinned-pinned non-uniform damped Rayleigh beam under the influence of a harmonic moving load for different mass ratio values

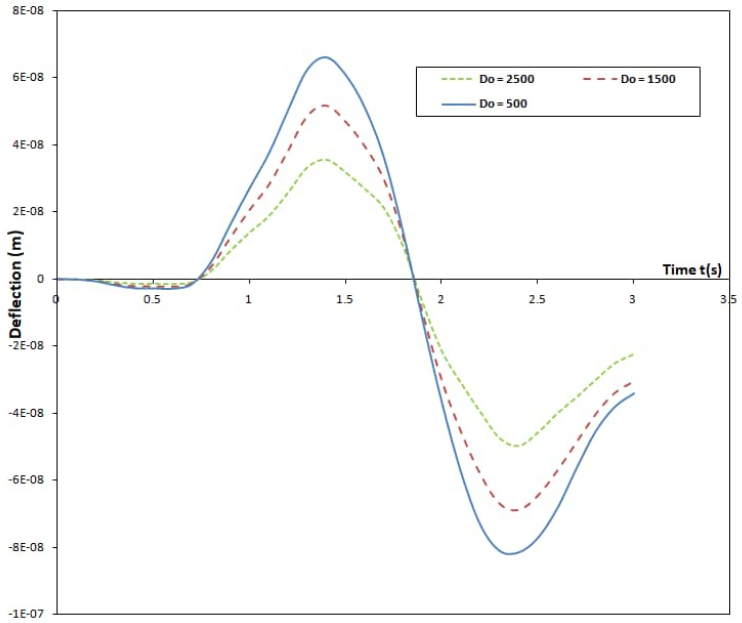

Figure 7:

The deflection profile of the moving force system's pinned-pinned non-uniform damped Rayleigh beam under the influence of a harmonic moving load for different damping coefficient values

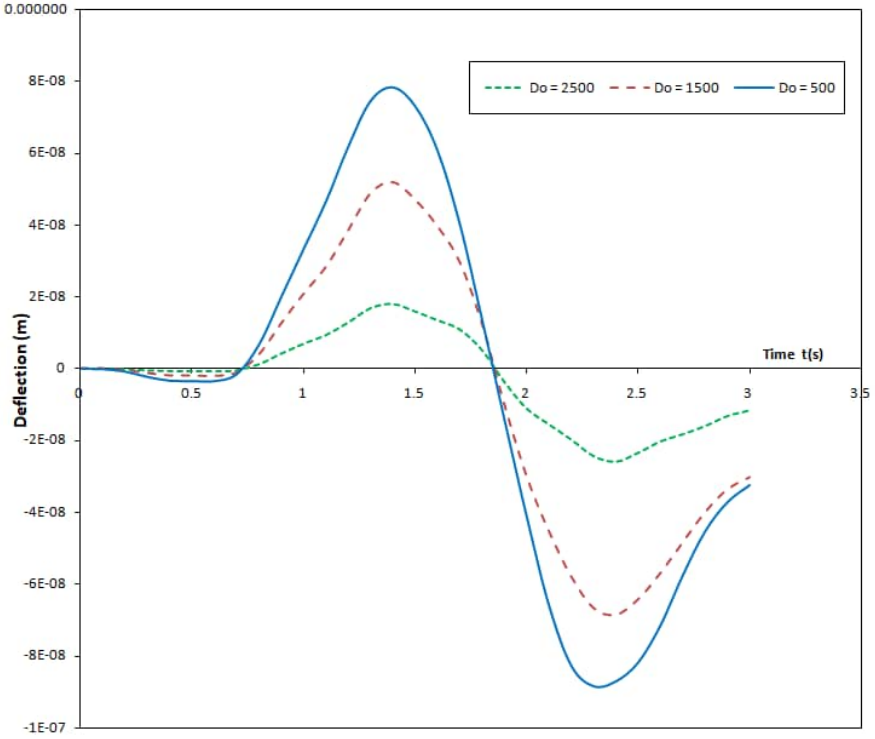

Figure 8:

The deflection profile of the moving mass system's pinned-pinned non-uniform damped Rayleigh beam under the influence of a harmonic moving load for different damping coefficient values

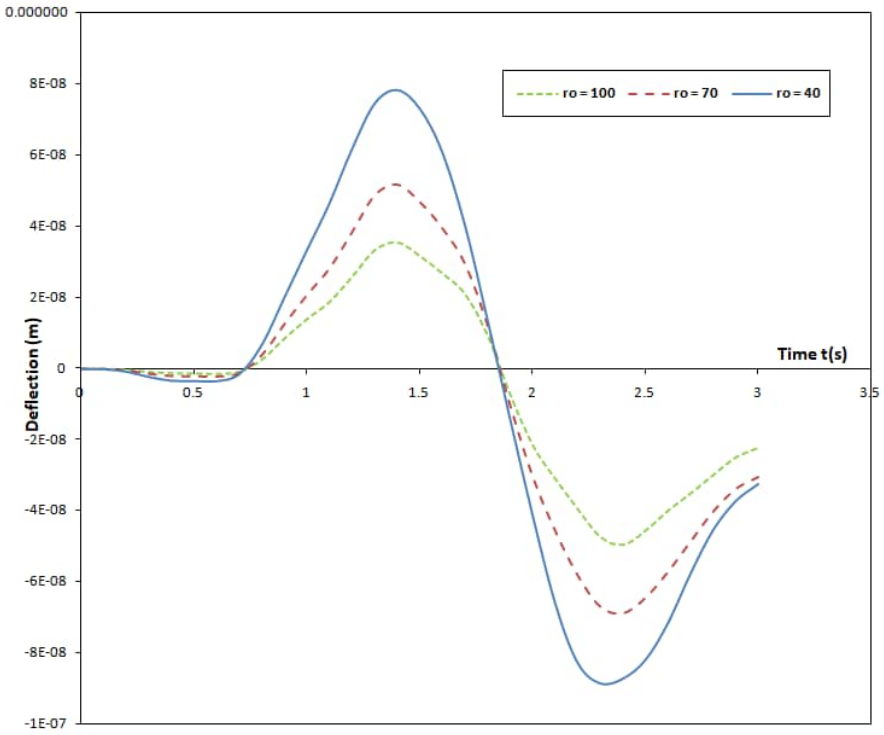

Figure 9:

The deflection profile of the moving force system's pinned-pinned non-uniform damped Rayleigh beam under the influence of a harmonic moving load for different rotatory inertia values

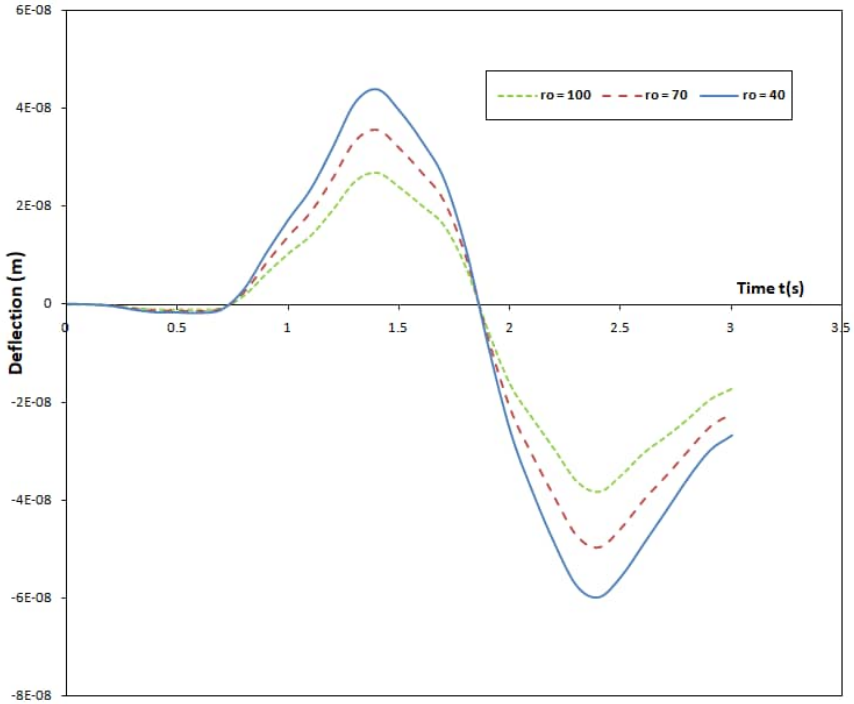

Figure 10:

The deflection profile of the moving mass system's pinned-pinned non-uniform damped Rayleigh beam under the influence of a harmonic moving load for different rotatory inertia values

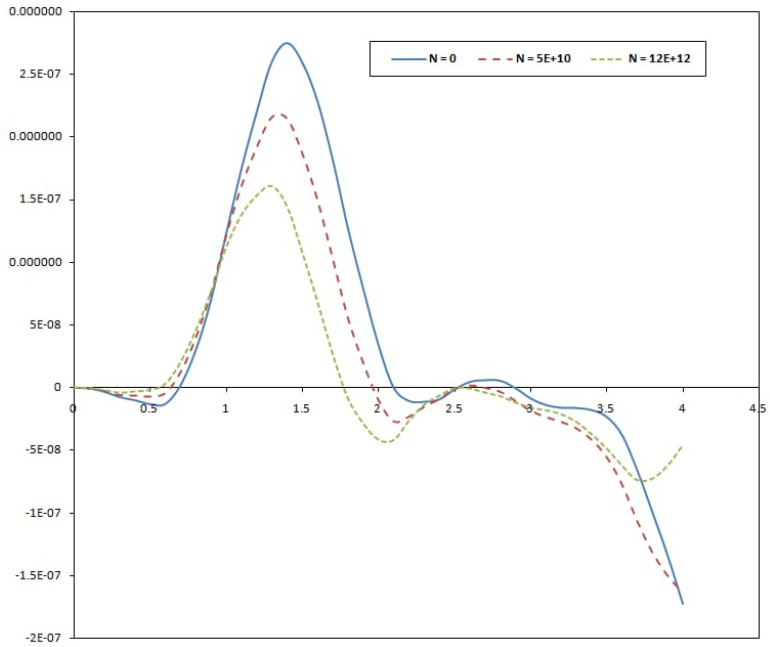

Figure 11:

The deflection profile of the moving force system's pinned-pinned non-uniform damped Rayleigh beam under the influence of a harmonic moving load for different axial force values

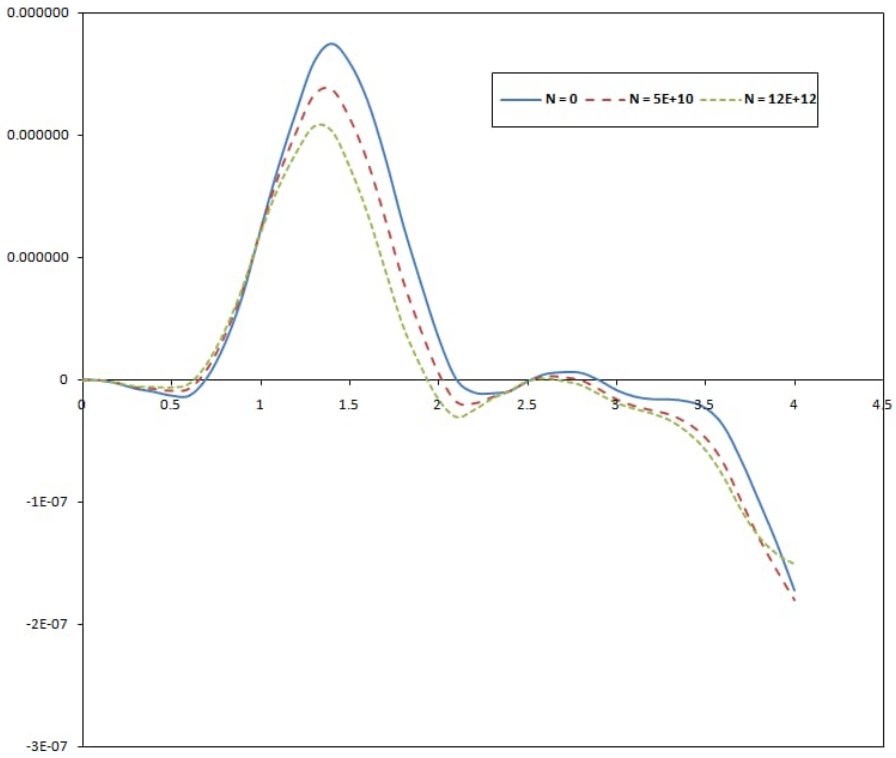

Figure 12:

The deflection profile of the moving mass system's pinned-pinned non-uniform damped Rayleigh beam under the influence of a harmonic moving load for different axial force values

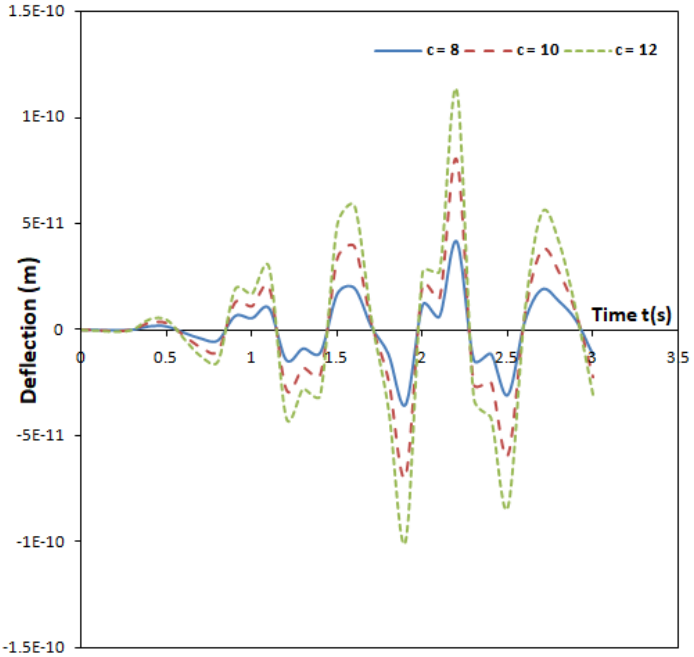

Figure 13:

The deflection profile of the moving force system's fixed-fixed non-uniform damped Rayleigh beam under the influence of a harmonic moving load for different speed values

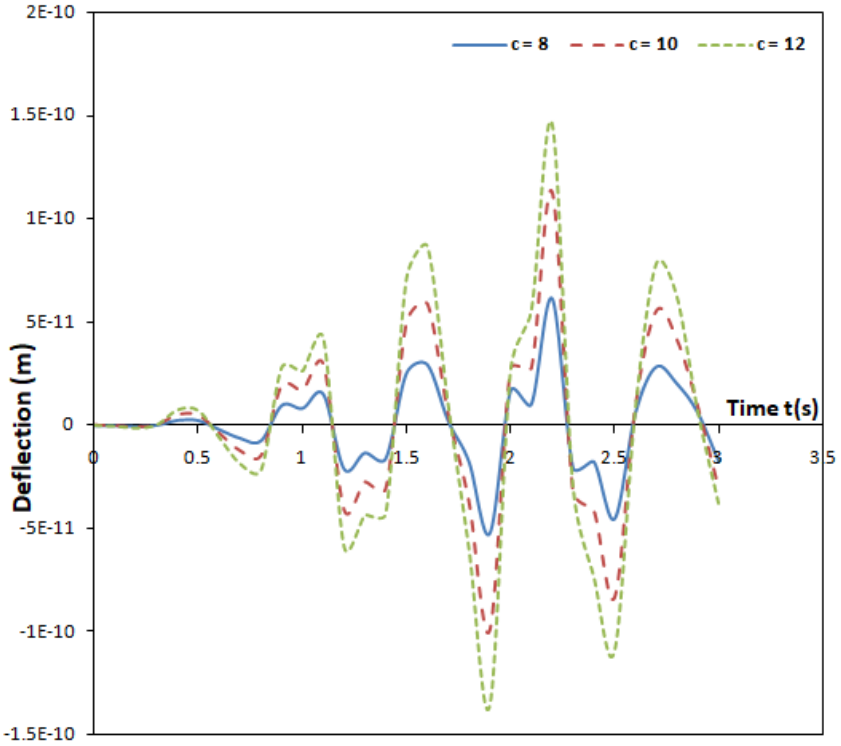

Figure 14:

The deflection profile of the moving mass system's fixed-fixed non-uniform damped Rayleigh beam under the influence of a harmonic moving load for different speed values

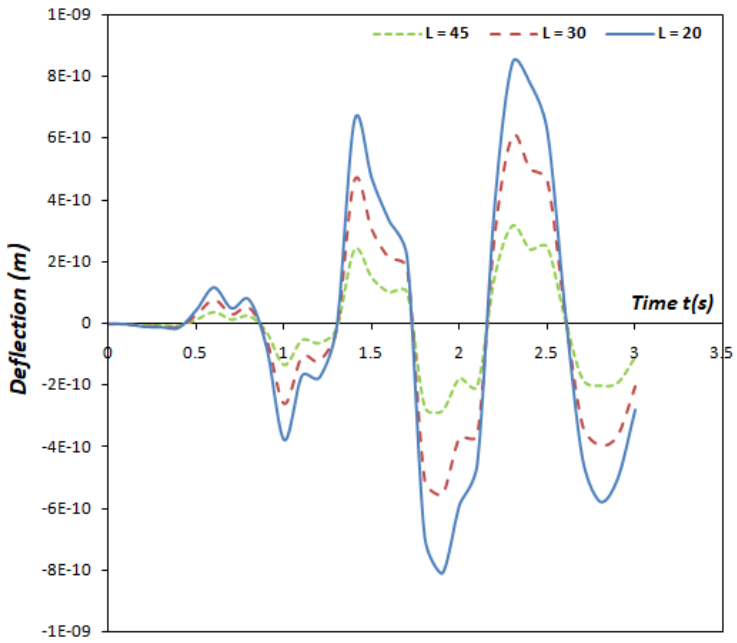

Figure 15:

The deflection profile of the moving force system's fixed-fixed non-uniform damped Rayleigh beam under the influence of a harmonic moving load for different Lenght values

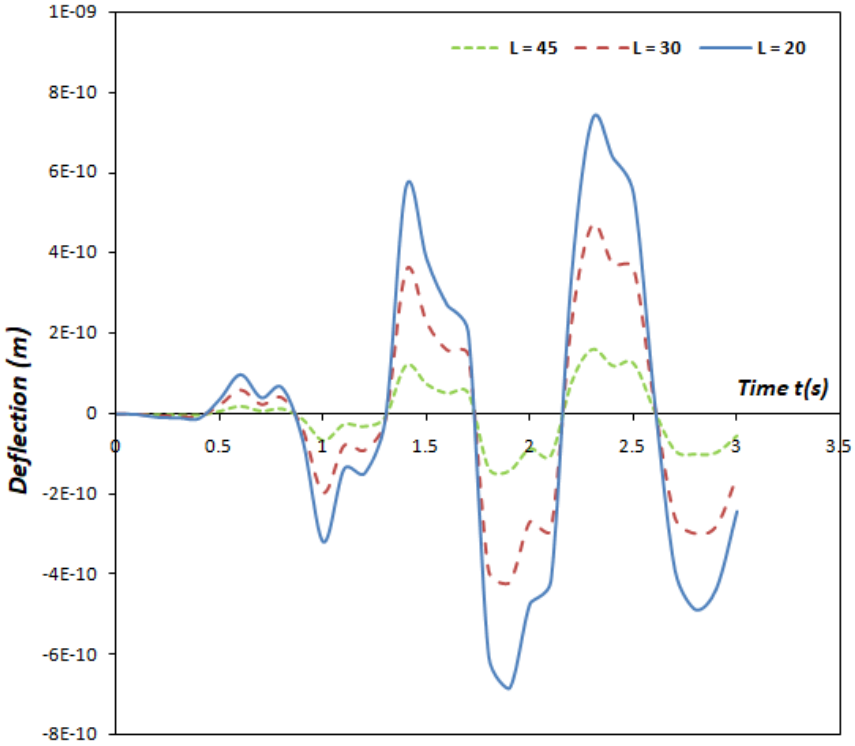

Figure 16:

The deflection profile of the moving mass system's fixed-fixed non-uniform damped Rayleigh beam under the influence of a harmonic moving load for different Lenght values

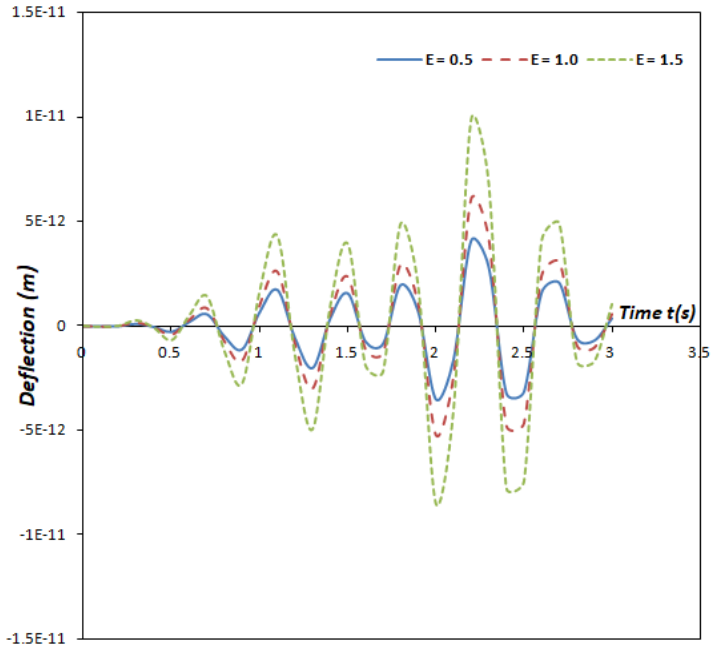

Figure 17:

The deflection profile of the moving force system's fixed-fixed non-uniform damped Rayleigh beam under the influence of a harmonic moving load for different mass ratio values

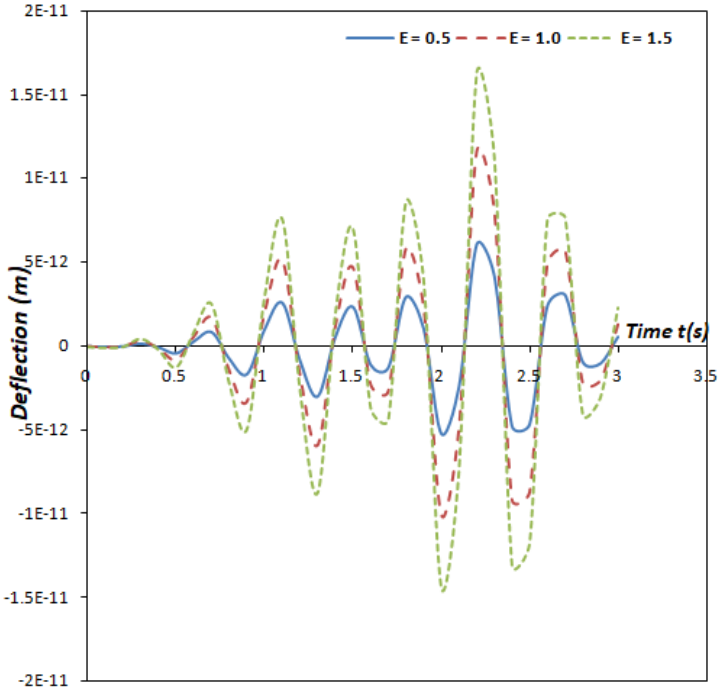

Figure 18:

The deflection profile of the moving mass system's fixed-fixed non-uniform damped Rayleigh beam under the influence of a harmonic moving load for different mass ratio values

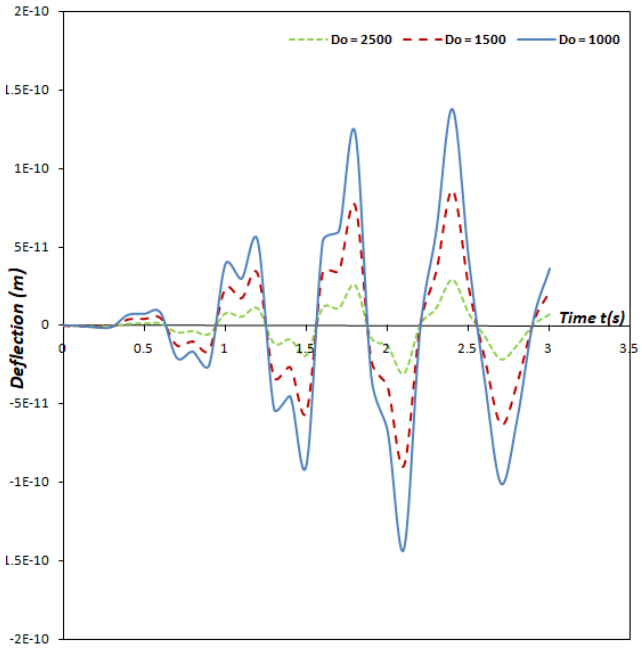

Figure 19:

The deflection profile of the moving force system's fixed-fixed non-uniform damped Rayleigh beam under the influence of a harmonic moving load for different damping coefficient values

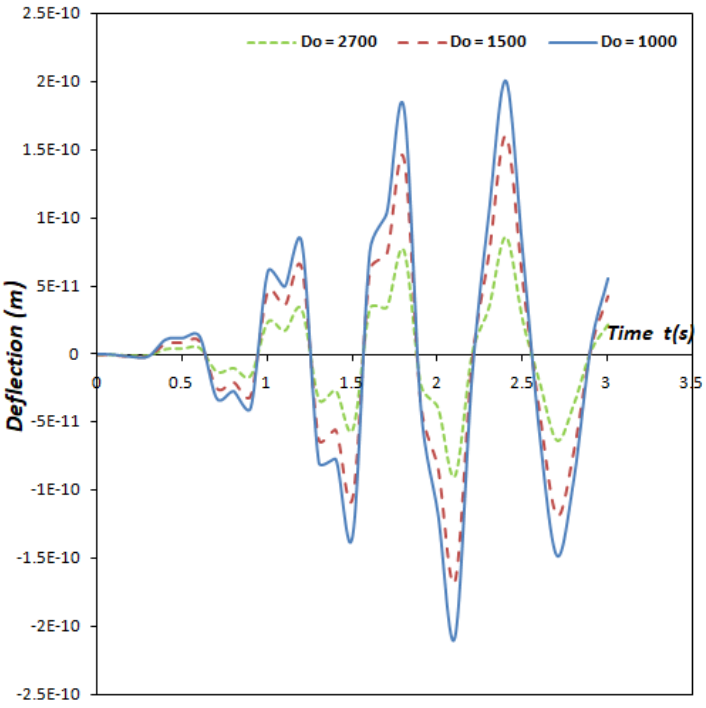

Figure 20:

The deflection profile of the moving mass system's fixed-fixed non-uniform damped Rayleigh beam under the influence of a harmonic moving load for different damping coefficient values

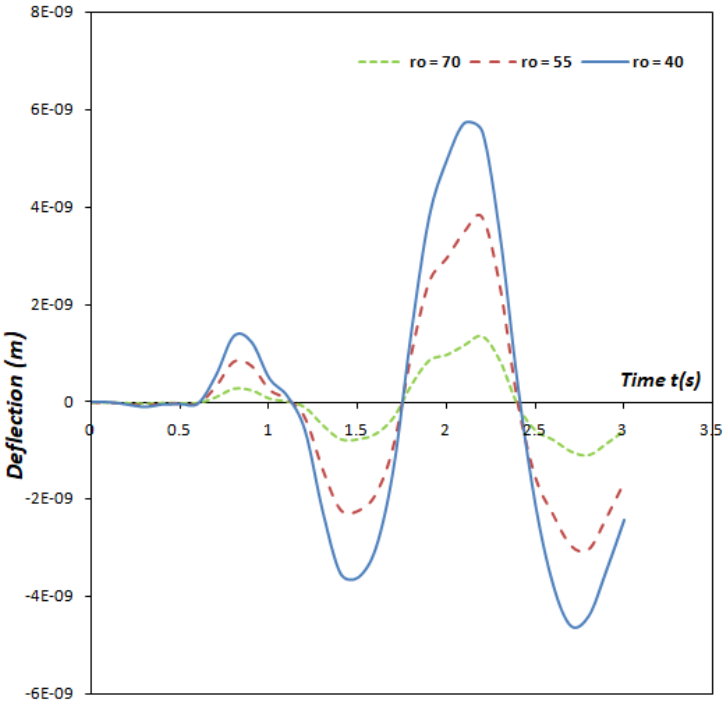

Figure 21:

The deflection profile of the moving force system's fixed-fixed non-uniform damped Rayleigh beam under the influence of a harmonic moving load for different rotatory inertia values

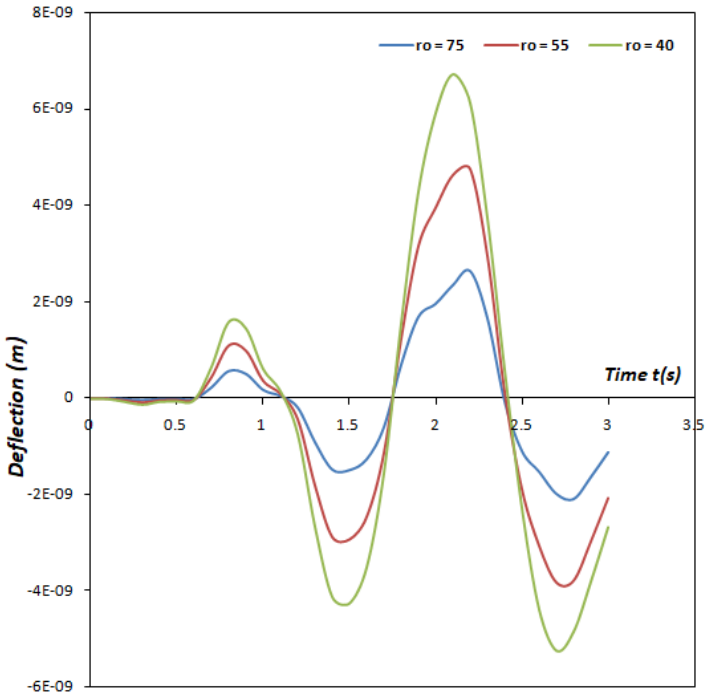

Figure 22:

The deflection profile of the moving mass system's fixed-fixed non-uniform damped Rayleigh beam under the influence of a harmonic moving load for different rotatory inertia values

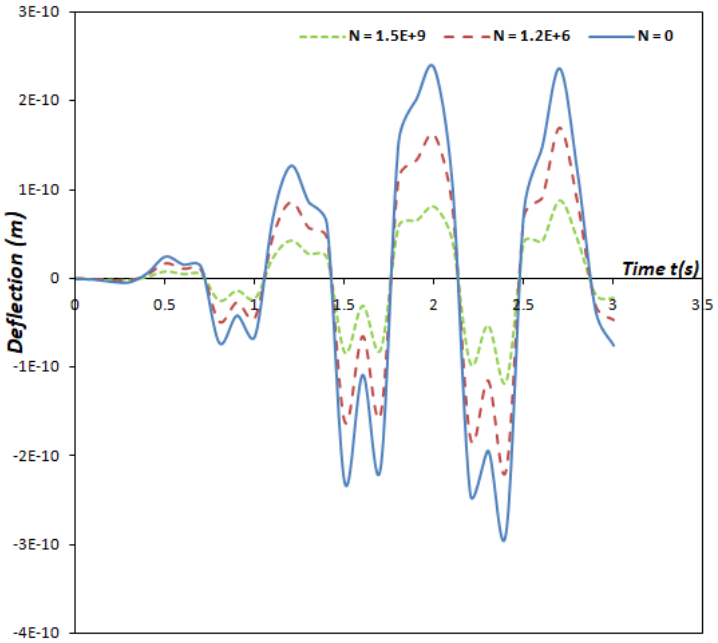

Figure 23:

The deflection profile of the moving force system's fixed-fixed non-uniform damped Rayleigh beam under the influence of a harmonic moving load for different axial force values

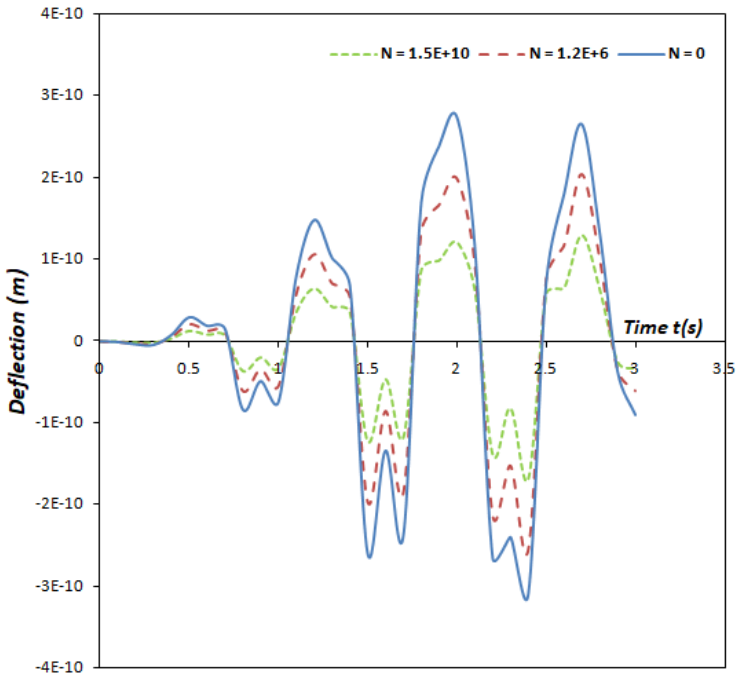

Figure 24:

The deflection profile of the moving mass system's fixed-fixed non-uniform damped Rayleigh beam under the influence of a harmonic moving load for different axial force values

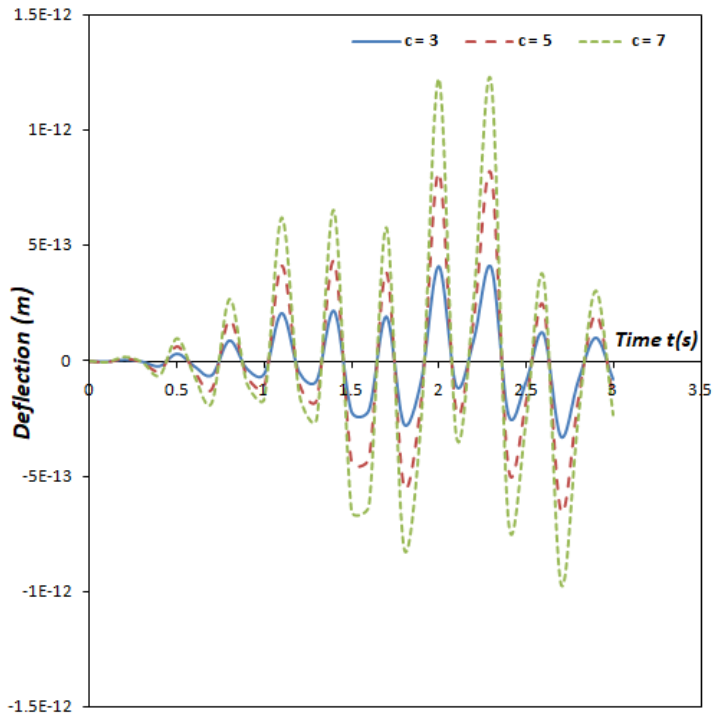

Figure 25:

The deflection profile of the moving force system's fixed-free non-uniform damped Rayleigh beam under the influence of a harmonic moving load for different speed values

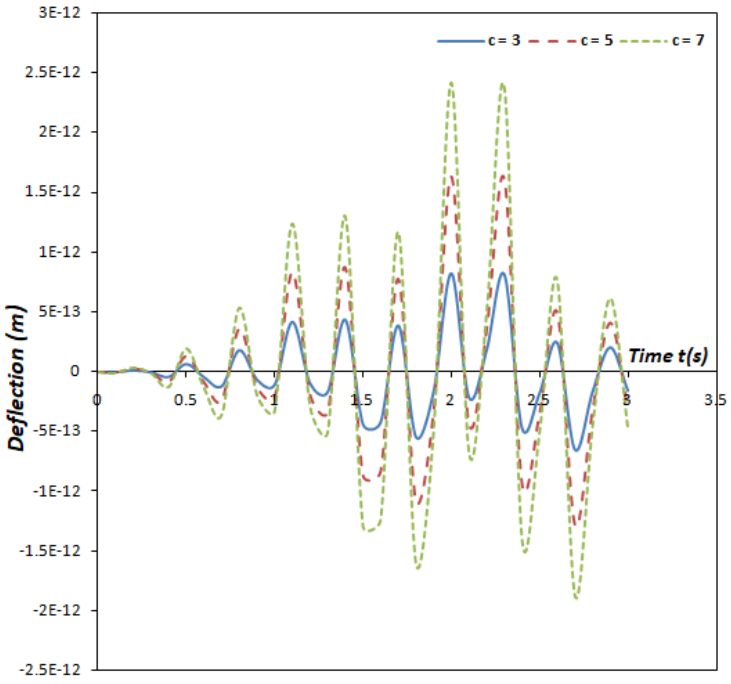

Figure 26:

The deflection profile of the moving mass system's fixed-free non-uniform damped Rayleigh beam under the influence of a harmonic moving load for different speed values

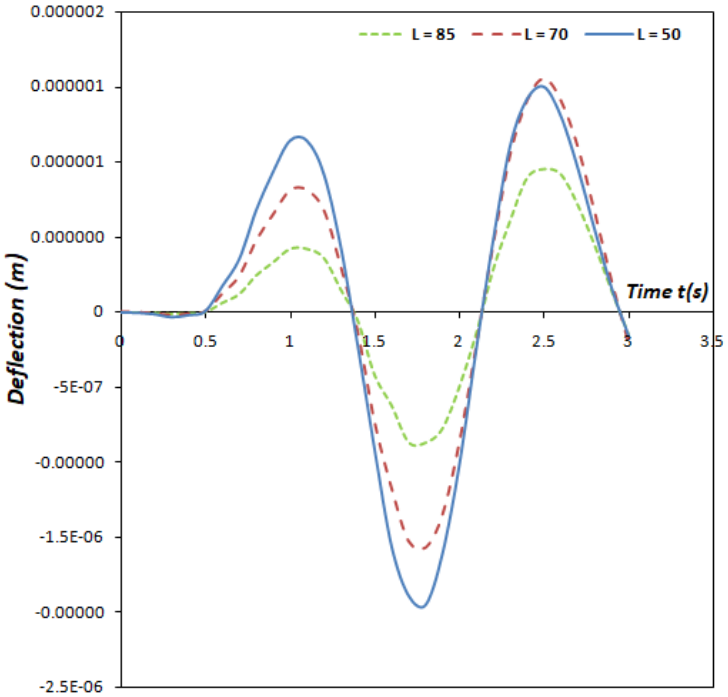

Figure 27:

The deflection profile of the moving force system's fixed-free non-uniform damped Rayleigh beam under the influence of a harmonic moving load for different Lenght values

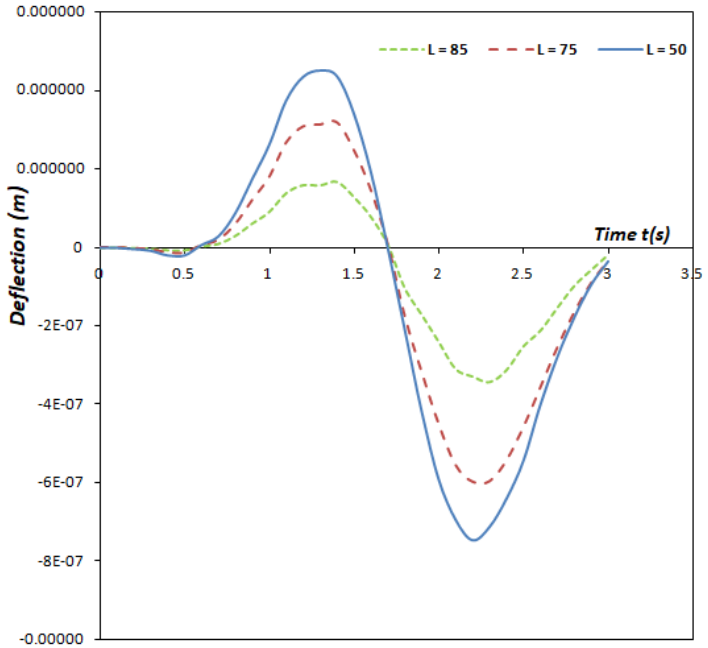

Figure 28:

The deflection profile of the moving mass system's fixed-free non-uniform damped Rayleigh beam under the influence of a harmonic moving load for different Lenght values

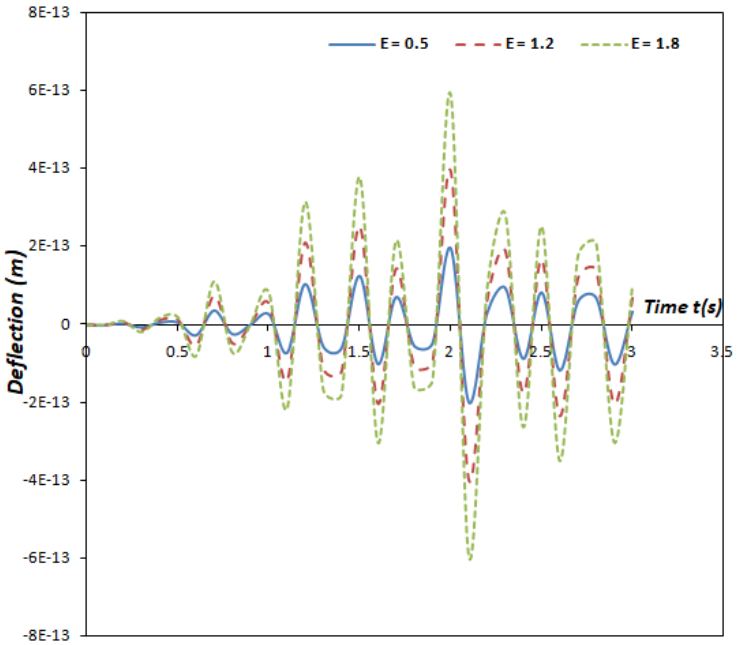

Figure 29:

The deflection profile of the moving force system's fixed-free non-uniform damped Rayleigh beam under the influence of a harmonic moving load for different mass ratio values

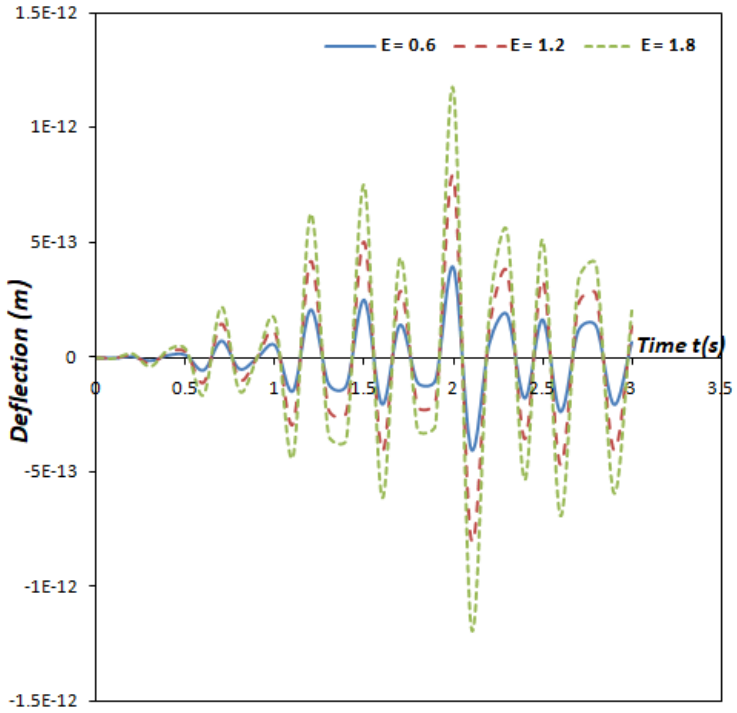

Figure 30:

The deflection profile of the moving mass system's fixed-free non-uniform damped Rayleigh beam under the influence of a harmonic moving load for different mass ratio values

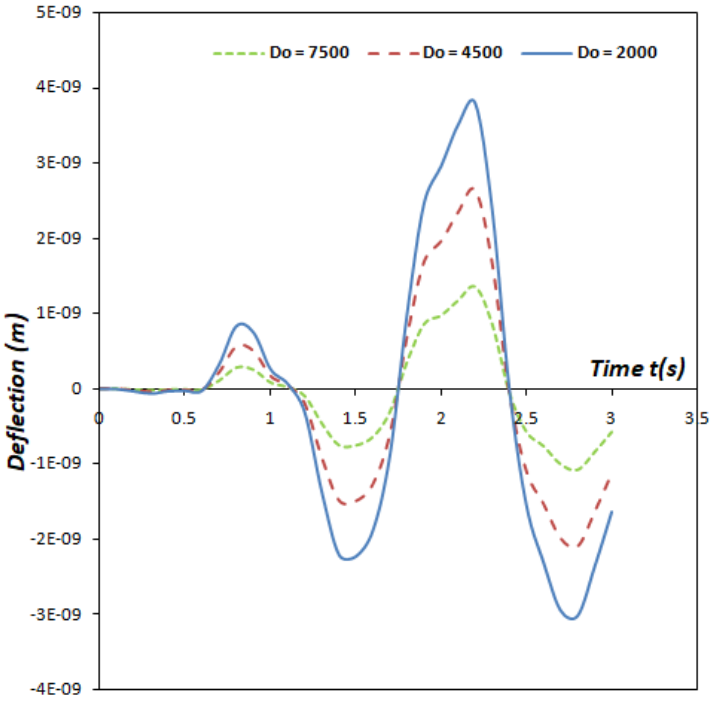

Figure 31:

The deflection profile of the moving force system's fixed-free non-uniform damped Rayleigh beam under the influence of a harmonic moving load for different damping coefficient values

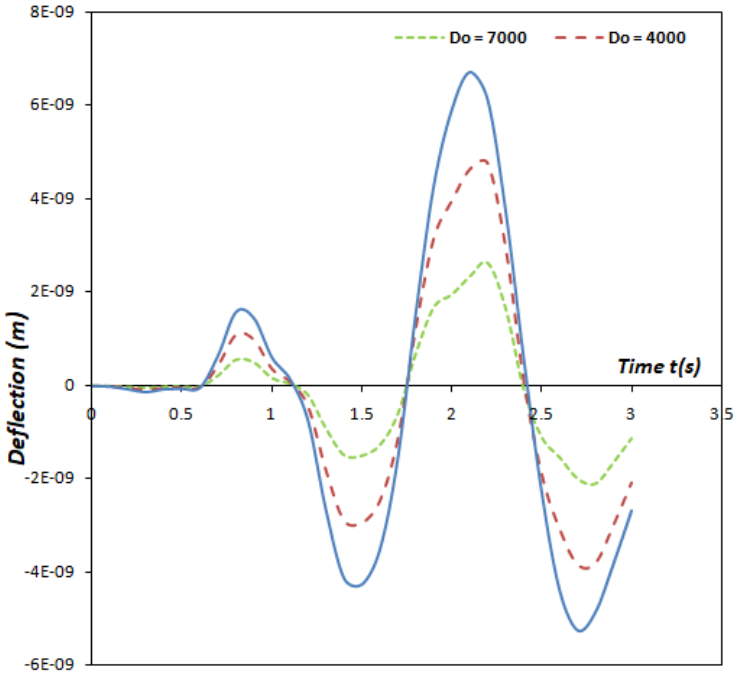

Figure 32:

The deflection profile of the moving mass system's fixed-free non-uniform damped Rayleigh beam under the influence of a harmonic moving load for different damping coefficient values

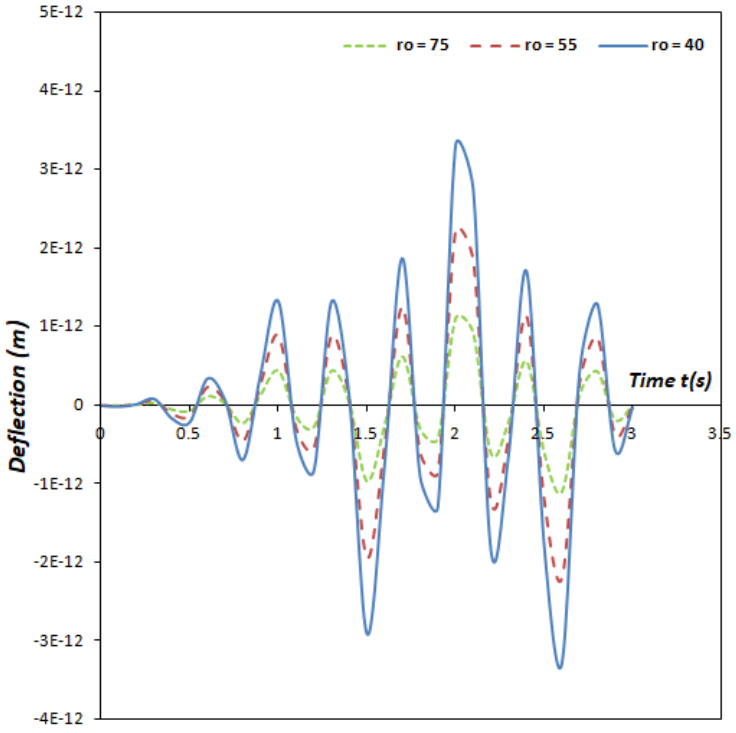

Figure 33:

The deflection profile of the moving force system's fixed-free non-uniform damped Rayleigh beam under the influence of a harmonic moving load for different rotatory inertia values

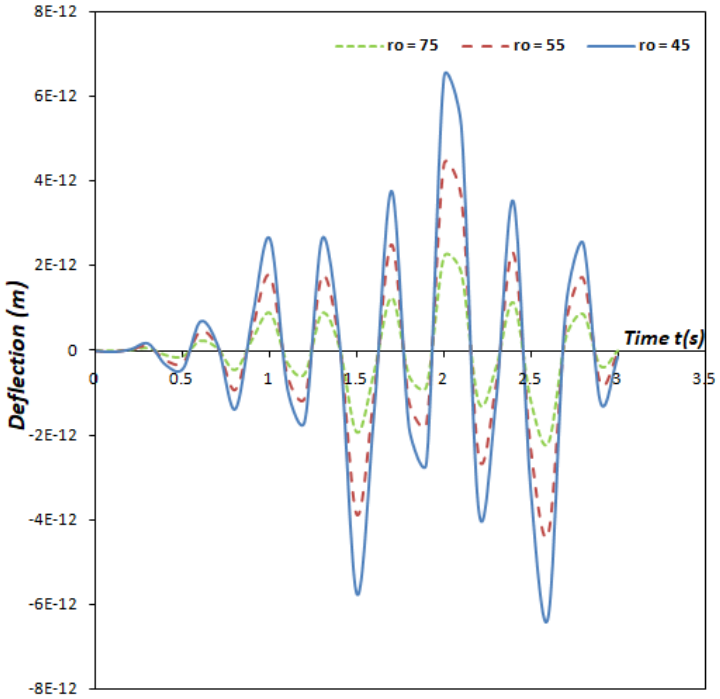

Figure 34:

The deflection profile of the moving mass system's fixed-free non-uniform damped Rayleigh beam under the influence of a harmonic moving load for different rotatory inertia values

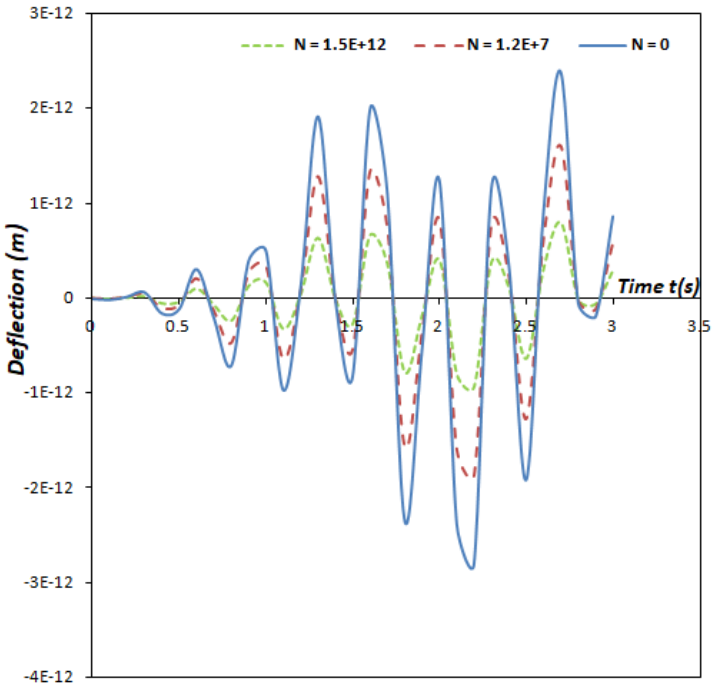

Figure 35:

The deflection profile of the moving force system's fixed-free non-uniform damped Rayleigh beam under the influence of a harmonic moving load for different axial force values

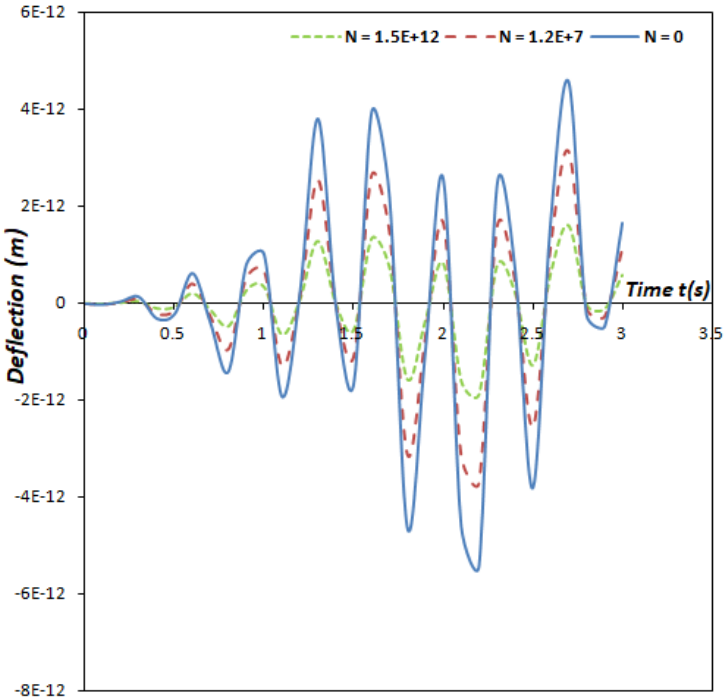

Figure 36:

The deflection profile of the moving mass system's fixed-free non-uniform damped Rayleigh beam under the influence of a harmonic moving load for different axial force values

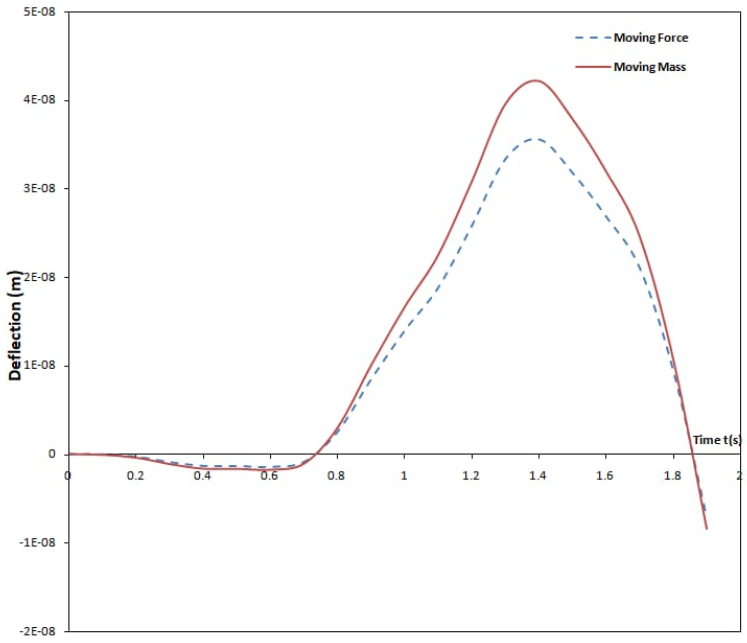

Figure 37:

Transverse deflection of the non-uniform damped Rayleigh beam for moving force and moving mass

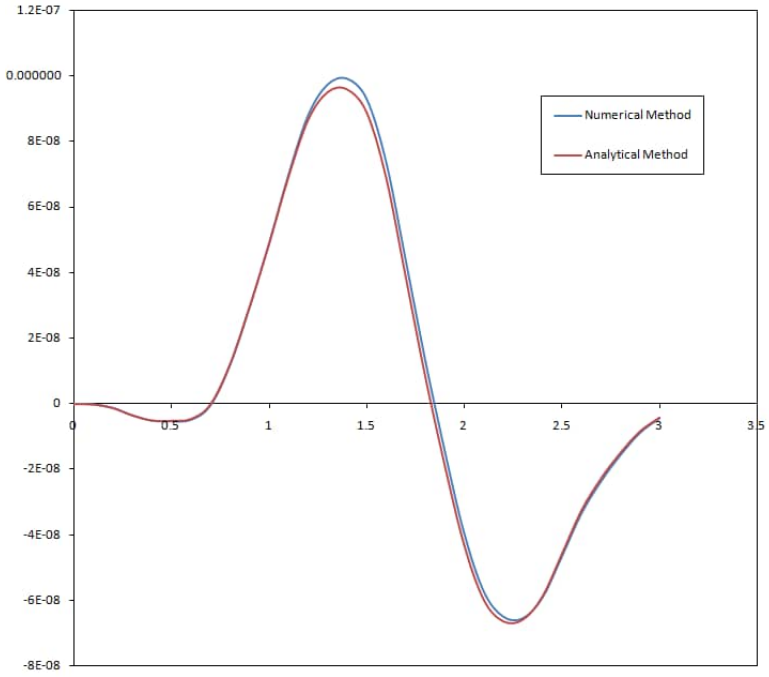

Figure 38:

Comparison of the analytical and numerical solution

Figures 35 and 36 illustrate the dynamic deflections of the beam under harmonic moving forces and masses, respectively, with $\xi = 2.5$, $D_o = 1500$, and varying N values. The response amplitude decreases as N increases. Figure 37 presents a comparative analysis of the transverse displacement of a non-uniform damped Rayleigh beam system under harmonic moving forces and masses. A key observation from this figure is that the deflection caused by the moving mass is substantially higher than that induced by the moving force. Consequently, resonance occurs earlier in the moving force system than in the moving mass system. Figure 38 presents a comparative study between the analytical and numerical solutions for the dynamic response of a non-uniform damped Rayleigh beam system. The results show an excellent correlation between the two solutions, with the numerical solution obtained using the Runge-Kutta method closely matching the analytical solution. The dynamic response of non-uniform damped Rayleigh beams on exponentially decaying foundations subjected to harmonic moving loads is significantly influenced by various parameters. Specifically, increasing speed leads to an exponential rise in deflection. Conversely, augmenting damping, rotatory inertia, and axial force serves to mitigate deflection, yielding more robust structures. Notably, this trend holds consistent across all three boundary conditions considered, namely pinned-pinned, fixed-fixed, and fixed-free. These findings have significant implications for the design, construction, and maintenance of various structures, including bridges, buildings, and machines, founded on exponentially decaying foundations. Optimizing beam properties and implementing vibration control measures are essential to ensure structural safety and integrity under dynamic loads. The proposed model has numerous real-world applications in structural engineering, particularly in the design and analysis of transportation infrastructure, buildings, industrial structures, and energy infrastructure. For instance, it can be used to analyze bridge response to moving loads, wind, and seismic forces, as well as highway pavement response to traffic loading and railway track response to train loading. This study demonstrates the practical relevance of the proposed model in structural engineering, highlighting its potential to inform the design and analysis of various structures, including buildings, industrial structures, and energy infrastructure. By providing insights into the dynamic response of non-uniform damped Rayleigh beams, this research contributes to the development of more robust and resilient structures that can withstand dynamic loads.

6 Conclusion

This investigation presents a comprehensive dynamic analysis of a non-uniform damped Rayleigh beam resting on an exponentially decaying foundation, subjected to harmonic moving loads. Employing the Generalized Galerkin Method (GGM), the governing fourth-order partial differential equations are transformed into a second-order ordinary differential equation. Analytical solutions are obtained using the Laplace transform and convolution theorem for the moving force problem, while the Runge-Kutta

method of order four is utilized for the moving mass problem. A parametric study is conducted to examine the influence of vital loads and structural parameters, including load velocity, beam length, axial forces, damping coefficient, and mass ratio, on the dynamic response characteristics of the beam under three distinct boundary conditions: pinned-pinned, fixed-fixed, and fixed-free. The findings of this study demonstrate excellent agreement with existing research, underscoring its potential for practical applications in structural and bridge engineering.

References

[1] Awodola T, Awe B, Jimoh S. VIBRATION OF NON-UNIFORM BERNOULLI-EULER BEAM UNDER MOVING DISTRIBUTED MASSES RESTING ON PASTERNAK ELASTIC FOUNDATION SUBJECTED TO VARIABLE MAGNITUDE. 2023;.

[2] Omolofe B, Adara EO. Dynamic amplification factor and interactions of a beam under compressive axial force and load travelling at varying velocity. Forces in Mechanics. 2023;13:100241.

[3] Akintomide A, Awodola T. Dynamic Response to Moving Distributed Masses of Prestressed Orthotropic Cantilever Plate Resting on Variable Pasternak Elastic Foundation. International Journal of Applied and Computational Mathematics. 2023;9(6):120.

[4] Adeoye A, Adeloye T. Flexural Rigidity Influence on Dynamic Response of Orthoropic Rectangular Plate Resting on Constant Elastic Foundation. Saudi J Civ Eng. 2024;8(7):140–158.

[5] Abouelregal AE, Ahmad H, Gepreeld KA, Thounthong P. Modelling of vibrations of rotating nanoscale beams surrounded by a magnetic field and subjected to a harmonic thermal field using a state-space approach. The European Physical Journal Plus. 2021;136(3):1–23.

[6] Oni S, Ogunbamike O. Dynamic Behaviour Of Non-Prismatic Rayleigh Beam On Pasternak Foundation And Under Partially Distributed Masses Moving At Varying Velocities. Journal of the Nigerian Mathematical Society. 2014;33(1-3):285–310.

[7] Ogunlusi T, Awodola T. Dynamic Behaviour of Simply Supported Non-Uniform Rayleigh Beam under Variable-Magnitude Accelerating Masses and Resting on Non-Uniform Bi-parametric Foundation. Asian Research Journal of Mathematics. 2024;20(11).

[8] Sarkar K, Ganguli R, Elishakoff I. Closed-form solutions for non-uniform axially loaded Rayleigh cantilever beams. Struct Eng Mech. 2016;60(3):455–470.

[9] Oni S, Ayankop-Andi E. ON THE RESPONSE OF A SIMPLY SUPPORTED NON-UNIFORM RAYLEIGH BEAM TO TRAVELLING DISTRIBUTED LOADS. Journal of the Nigerian Mathematical Society. 2017;36(2):435–457.

[10] Mahapatra K, Panigrahi S. Dynamic response of a damped Euler–Bernoulli beam having elastically restrained boundary supports. Journal of the Institution of Engineers (India): Series C. 2019;100:891–905.

[11] Adetunde I, Seidu B, Campus N. Dynamic response of loads on viscously damped axial force rayleigh beam. American Journal of Applied Sciences. 2008;5(9):1110–1116.

[12] Akinpelu FO. The response of viscously damped Euler-Bernoulli beam to uniform partially distributed moving loads. Applied Mathematics. 2012;3(3):199–204.

[13] Alimi A, Adekunle J. Dynamics analysis of a damped non uniform beam subjected to loads moving with variable velocity. Archives of Current Research International. 2018;13(2):1–16.

[14] Ogunlusi T, Awodola T, Ikare J, Okafor N. Dynamic Behaviours of Non-Uniform Rayleigh Beam under Variable-Magnitude Accelerating Masses and Resting on Non-Uniform Bi-parametric Foundation with General Boundary Conditions;.

[15] Tolorunshagba J. Response to moving variable concentrated load of non-uniform beams resting on exponentially decaying foundation. Journal of Emerging Trends in Engineering and Applied Sciences. 2014;5(6):378–383.

[16] Adekunle JS, Folakemi AO. Dynamic Response of Non-Uniform Elastic Structure Resting on Exponentially Decaying Vlasov Foundation under Repeated Rolling Concentrated Loads;.

[17] Simões F, da Costa AP. Finite element steady state solution of a beam on a frictionally damped foundation under a moving load. International Journal of Non-Linear Mechanics. 2019;117:103247.

[18] Froio D, Rizzi E, Simões FM, Da Costa AP. Universal analytical solution of the steady-state response of an infinite beam on a Pasternak elastic foundation under moving load. International Journal of Solids and Structures. 2018;132:245–263.

[19] Fryba L. Vibration of solids and structures under moving loads, the netherlands: Noordhoff International. Groningen;.

[20] Taha MH, Abohadima S. Mathematical model for vibrations of non-uniform flexural beams. Engineering Mechanics. 2008;15(1):3–11.

[21] Omolofe B, Adedowole A, Ajibola S, Ahmed J. Exact Vibration Solution for initially stressed Beams resting on Elastic Foundation and subjected to partially distributed masses. Journal of the Nigerian Association of Mathematical Physics. 2011;18:91–98.